Transient Nonlinear Rayleigh-Bénard Convection with Single-Mode Initiation

Peder A. Tyvand[1] and Jonas Kristiansen Nøland[2]
[1)]*Norwegian University of Life Sciences (NMBU), 1432 Ås, Norway, Tlf.: +47-67231564.*
[2)]*Norwegian University of Science and Technology (NTNU), 7034 Trondheim, Norway, Tlf.: +47-73594202.*

(*Electronic mail: Peder.Tyvand@nmbu.no.)

(Dated: 29 October 2021)

Transient nonlinear convection in a finite Prandtl number fluid heated uniformly from below is studied analytically and numerically. We consider the simple geometry of a square cavity with normal-mode compatible boundary conditions. By design, only the marginal state of convection onset contributes to the initial condition for the two-dimensional supercritical convection. The thermal amplitude and the flow amplitude are taken as two independent initial conditions. There are two ways of initiation: (i) Soft start with very small initial amplitude, leading to early exponential growth. (ii) Kick-started transient convection with relatively large initial amplitudes, by which we perform a small-time expansion for benchmarking. Seemingly complicated transient flow occurs with a kick-start where the initial spin and the initial buoyancy torque are in conflict. However, the intricate spiraling flow decays after a couple of reversals of flow directions, and a steady convection settles. This is due to the strict antisymmetry of the temperature perturbation around the mid-point of the cavity, in combination with the symmetry of the flow field.

I. INTRODUCTION

Fluid mechanics belongs to deterministic continuum physics. A broad access to first-principle nonlinear phenomena gives fluid mechanics a lasting scientific impact. Basic nonlinearities of fluid flows are studied with good conceptual clarity and relatively precise computational and experimental tools. Nonlinear Rayleigh-Bénard convection has earned a central place in nonlinear fluid mechanics, encompassing a diversity of phenomena with gradual routes to chaos.

The concept of self-organization by hierarchies of instabilities may be traced back to Turing[1]. A much broader approach based on nonlinear theory was popularized by Prigogine and Stengers[2]. Rayleigh-Bénard convection is a key phenomenon in this cross-disciplinary research. Supercritical Rayleigh-Bénard convection may be caused either by designed initiation or by noise. The linear theory of selection of a preferred marginally unstable flow from arbitrary disturbances has proven to be a fruitful approach. Its stability criterion is supported by experiments.

Our idea is to let transient supercritical Rayleigh-Bénard convection evolve from initial states that are as elementary as possible. The problem of convection onset by selection from arbitrary disturbances remains important, while the notion of successive supercritical instabilities will be put aside in the present paper. We will focus on nonlinear convection as initial value problems, taking the preferred thermomechanical Fourier mode from the linearized onset problem as the single initial pair of modes. Higher Fourier modes will evolve naturally in time by nonlinear self-interactions.

The stability theory for a fluid layer heated uniformly from below was developed by Rayleigh[3]. The theory of finite-amplitude supercritical convection was pioneered by Malkus and Veronis[4], calculating the flow amplitude and heat transfer as functions of the supercritical Rayleigh number. Chandrasekhar[5] gave the Rayleigh-Bénard problem a central role in his treatise on linear stability theory for hydrodynamics and hydromagnetic flows. Moore and Weiss[6] studied two-dimensional nonlinear convection for very high Rayleigh numbers and identified transitions between steady and oscillatory convection. Among many review articles of the classical theory of nonlinear Rayleigh-Bénard convection we refer to Palm[7] and Busse and Clever[8]. The monograph by Drazin and Reid[9] placed this established theory of nonlinear thermal convection into the broad perspective of hydrodynamic stability theory.

The Rayleigh-Bénard problem stands out with mathematical simplicity in the theory of hydrodynamic stability. Its mathematical simplicity comes from the fact that its basic unperturbed state is a trivial finite-amplitude solution with a uniform temperature gradient. Other basic states of hydrodynamic stability are more complicated solutions to nonlinear problems. Nonlinearities in the full mathematical problem are needed to link the basic state to its perturbations, since a fully linearized problem could not support any stability analysis.

The present work is devoted to the role of initial conditions in the supercritical Rayleigh-Bénard problem. It will be studied by linear theory, weakly nonlinear theory as well as strongly nonlinear theory. Since the pioneering work by Schlüter, Lortz and Busse[10], the focus of the analytical research of supercritical Rayleigh-Bénard convection has been on stability theory[11]. Initial value problems have played a secondary role in this context.

Nonlinear initial value problems for convection came in focus with the seminal work by Newell and Whitehead[12]. Normand *et al*.[13] followed up these ideas, carried further by Pomeau and Manneville[14]. Analogies with crystal structures inspired experimental work on pattern formations in supercritical convection, see e.g. Bodenschatz *et al*.[15], Cerisier *et al*.[16] and the book by Koschmieder[17]. Bestehorn and Haken[18] performed numerical simulations of supercritical convection patterns, based on dimension-reduced equations.

Finite Prandtl number is crucial for considering supercrit-

ical convection as an initial value problem since it offers two time-derivatives in the nonlinear mathematical problem. Thereby one also gets two independent initial conditions to play with, choosing different weighting of initial temperature perturbation versus initial flow. As a contrast, the limit of infinite Prandtl number includes only one time-derivative and is not rich enough for interesting transient nonlinear convection to be triggered by a single-mode initiation.

Nonlinear flow phenomena can be studied from three distinct perspectives.

(i) The causal perspective of identifying physical causes and classifying their qualitative and quantitative effects. The oscillations for small and moderate Prandtl numbers is a good example from Rayleigh-Bénard convection. Since the linearized stability problem does not allow any oscillatory behavior, these oscillations are exclusively nonlinear phenomena. The basic causality behind these oscillations remains a challenge, comprising the frequency spectra of these oscillations, and their dependencies on the Prandtl number and Rayleigh number. Moore and Weiss[6] addressed these questions, with the limitations of a finite-difference numerical scheme at an early stage of computational fluid mechanics. Their work is complemented by more recent papers[19,20] where two-dimensional nonlinear convection is studied with greater numerical accuracy.

(ii) The initiation perspective of considering nonlinear flows as mathematical initial value problems. This is the approach of weather forecast, where observations continuously update the initial conditions. A scientific approach of initiation is to specify the flow fully at the initial instant $t = 0$ and study its nonlinear evolution without interventions. The mathematical advantage with this approach is that the challenges of causality are circumvented, since one does not need to know anything about the flow before $t = 0$. We will present two distinct alternatives for initiating convection at a given supercritical Rayleigh number. The standard soft start is where small perturbations grow exponentially during an early stage. Our second alternative is the kick-started convection, where at least one amplitude starts with the same order of magnitude as the steady-state solution for the given supercritical Rayleigh number.

(iii) A third perspective is the selection mechanisms by instabilities, which has a lasting influence on the field of Rayleigh-Bénard convection. This perspective was first established by Lord Rayleigh[3], with his linearized stability analysis for the onset of convection. At the critical Rayleigh number, the single marginal state is naturally selected as the only mode of disturbance which does not decay but remains steady. The onset selection is understood by linear theory. It is not obvious how to settle selection principles for nonlinear theory, as they tend to be presented in an implicit manner[8]. Palm[21] presented an early selection theory for nonlinear hexagonal convection in a fluid with viscosity dependent on temperature. The gradually emerging selection principle of two successive instabilities to be established for nonlinear convection patterns. Busse[22] started this research, which grew from the seminal work of small-amplitude nonlinear convection by Schlüter, Lortz and Busse[10]. The idea of selecting hierarchies

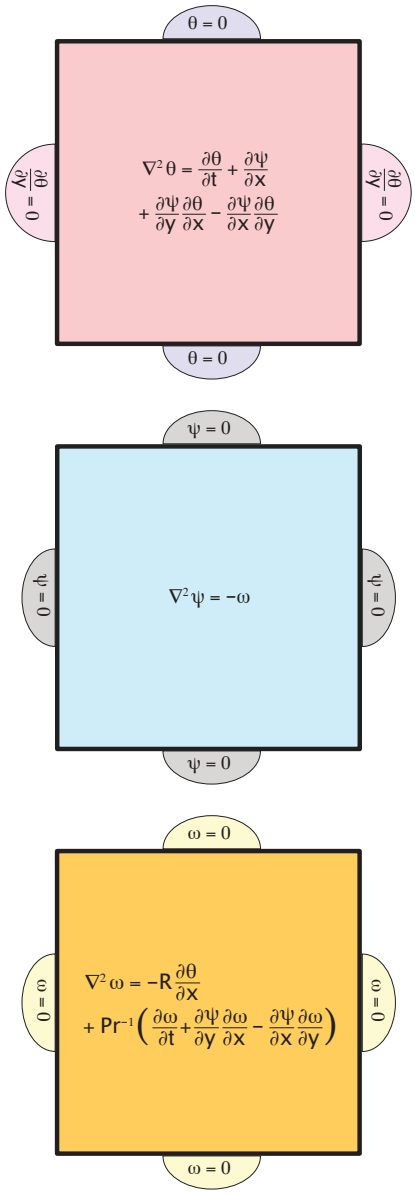

FIG. 1. Formulation of the spatially sixth-order time-dependent nonlinear Rayleigh-Bénard problem in a square cavity, in terms of three coupled Poisson equations for $\theta(x,y,t)$, $\psi(x,y,t)$ and $\omega(x,y,t)$. The homogeneous boundary conditions for two-dimensional convection in the unit square are of the Dirichlet type, with two exceptions: The thermal conditions along the insulating walls $x = 0$ and $x = 1$ are Neumann conditions.

of nonlinear flow modes from noise reached a state of maturity already three decades ago[8]. These authors pointed to the alternative of studying nonlinear convection as initial value problems, but they did not address the dilemma of designed initiation versus initial noise.

The stability domain ("Busse balloon") for steady convection is small when the Prandtl number is below one[8,9]. A notable limitation for this selection by successive instabilities is that one linearizes the time-dependent vortex interactions. One may circumvent these limitations by fully nonlinear simulations based on generic initiation modes. In this context, we launch the concept of kick-starting transient nonlinear convection from a minimalist set of initiation modes, which are generic by being hand-picked from linear theory. A small-time expansion will make it possible to trace the early evolution of this strongly nonlinear process. Our intention is to leave challenges for improved analytical understanding of transient nonlinear convection evolving from initial states with step-wise increments of complexity. The evolution towards chaos will be blocked and reversed by strict spatial symmetries in the present model. A natural next step will be to consider initial states without such symmetry constraints, which will increase the complexities of transient convection[23].

II. MATHEMATICAL FORMULATION

The standard dimensionless Boussinesq equations for buoyancy-driven convection in a Newtonian fluid are

$$\nabla \cdot \vec{v} = 0, \tag{1}$$

$$Pr^{-1}\left(\frac{\partial \vec{v}}{\partial t} + \vec{v}\cdot\nabla\vec{v}\right) + \nabla p = R\theta\vec{j} + \nabla^2\vec{v}, \tag{2}$$

$$\frac{\partial \theta}{\partial t} - v + \vec{v}\cdot\nabla\theta = \nabla^2\theta, \tag{3}$$

see Drazin and Reid[9]. The two dimensionless parameters are the Prandtl number Pr and the Rayleigh number R. These are defined by

$$Pr = \frac{\nu}{\kappa}, \quad R = \frac{g\alpha d^3\Delta T}{\nu\kappa}. \tag{4}$$

The velocity field is $\vec{v}$, while p and θ denotes the perturbations of pressure and temperature. Pr and R depend on the kinematic viscosity ν, the diffusivity κ, the thermal expansion coefficient α. ΔT is the temperature difference between the lower and upper boundary, and is taken as unit for dimensionless temperature difference. The Newtonian fluid layer with depth d is taken as unit for dimensionless length. d^2/κ is the unit of dimensionless time, while κ/d is the dimensionless velocity unit.

We consider only two-dimensional flow in the vertical x,y plane. The unit vectors are denoted by $\vec{i}$, $\vec{j}$ for the horizontal x direction and the vertical y direction, respectively. The corresponding Cartesian velocity components are denoted by (u,v). We will apply the classical conditions of impermeable, stress-free and perfectly conducting boundaries

$$v = \frac{\partial^2 v}{\partial y^2} = \theta = 0, \text{ at } y = 0 \text{ and } y = 1. \tag{5}$$

A. Formulation in terms of the streamfunction

We express the velocity vector $\vec{v}$ by the streamfunction ψ

$$(u,v) = \left(\frac{\partial \psi}{\partial y}, -\frac{\partial \psi}{\partial x}\right), \tag{6}$$

so that the continuity equation (1) is satisfied. The vorticity field ω is

$$\omega = \frac{\partial v}{\partial x} - \frac{\partial u}{\partial y} = -\nabla^2\psi. \tag{7}$$

We take the curl of the momentum equation (2) to get the nonlinear vorticity equation

$$Pr^{-1}\left(\frac{\partial \omega}{\partial t} + \frac{\partial \psi}{\partial y}\frac{\partial \omega}{\partial x} - \frac{\partial \psi}{\partial x}\frac{\partial \omega}{\partial y}\right) = R\frac{\partial \theta}{\partial x} + \nabla^2\omega. \tag{8}$$

The nonlinear heat equation (3) can be written

$$\frac{\partial \theta}{\partial t} + \frac{\partial \psi}{\partial x} + \frac{\partial \psi}{\partial y}\frac{\partial \theta}{\partial x} - \frac{\partial \psi}{\partial x}\frac{\partial \theta}{\partial y} = \nabla^2\theta. \tag{9}$$

These are the full nonlinear equations.

The boundary conditions (5) are preferably rewritten as follows

$$\psi = \omega = \theta = 0, \text{ at } y = 0 \text{ and } y = 1. \tag{10}$$

In Figure 1 we sketch a square cavity filled with fluid. The three coupled sets of nonlinear governing equations in two dimensions are displayed, together with the respective boundary conditions. The square cavity is to be introduced later in the text, together with its sidewall conditions compatible with normal modes.

III. STANDARD LINEAR THEORY

We will first give the general normal mode theory of onset in terms of Cartesian coordinates. An eigenvalue problem with full degeneracy due to its normal mode type of eigenfunctions is convenient when we study slightly supercritical convection. The eigenvalue problem for the onset of convection is independent of the Prandtl number[5], with a non-oscillatory marginal state.

The full linearized version of the governing equations (8) - (9) is

$$Pr^{-1}\frac{\partial \omega}{\partial t} = R\frac{\partial \theta}{\partial x} + \nabla^2\omega, \tag{11}$$

$$\frac{\partial \theta}{\partial t} + \frac{\partial \psi}{\partial x} = \nabla^2 \theta, \tag{12}$$

recalling the relationship $\omega = -\nabla^2 \psi$. The stationary eigenvalue problem may be represented by two equivalent equations

$$R^{-1}\nabla^6 \theta - \frac{\partial^2 \theta}{\partial x^2} = 0, \qquad R^{-1}\nabla^6 v - \frac{\partial^2 v}{\partial x^2} = 0, \tag{13}$$

with the boundary conditions

$$\theta = \frac{\partial^2 \theta}{\partial y^2} = \frac{\partial^4 \theta}{\partial y^4} = v = \frac{\partial^2 v}{\partial y^2} = \frac{\partial^4 v}{\partial y^4} = 0, \text{ at } y = 0 \text{ and } y = 1. \tag{14}$$

The eigenfunctions for the temperature and the vertical velocity can be written,

$$\theta = A\sin(\pi y)\cos(kx), \qquad v = B\sin(\pi y)\cos(kx) = -\frac{\partial \psi}{\partial x}, \tag{15}$$

where the general normal-mode dependency $\sin(N\pi y)$ is represented only by its most unstable vertical mode $N = 1$. The temperature amplitude is A, while the corresponding velocity amplitude is denoted by B. The wave number k has a critical value given by $k = \pi/\sqrt{2}$ where the marginal Rayleigh number given by the general formula

$$R_{marginal}(k) = \frac{(\pi^2 + k^2)^3}{k^2}, \tag{16}$$

takes the critical value $R_{marginal}(\pi/\sqrt{2}) = 27\pi^4/4 = 657.511$, first derived by Rayleigh[3]. We note the general formula for the ratio between the amplitudes of the eigenfunctions

$$\frac{B}{A} = k^2 + \pi^2, \tag{17}$$

with the special value $B/A = (3/2)\pi^2$ for the preferred mode.

It is obvious that the dimensionless temperature is scaled appropriately with ΔT as a unit. The fact that the ratio B/A is of order 10 indicates that the chosen unit of dimensionless velocity is one order of magnitude smaller than the appropriate physical scaling for velocity. We note this apparent imbalance in thermomechanical scaling, which applies to the onset and to slightly supercritical convection. The situation may change when we consider supercritical convection for small Prandtl numbers since a finite Prandtl number influences any transient evolution of a supercritical flow. This influence is expected to be stronger the smaller the Prandtl number.

The role of the Rayleigh number is transparent according to linear theory. Once the critical Rayleigh number R_c has been identified for the preferred legal mode of disturbance, we can introduce $\Delta R = R - R_c$ as the difference between the actual Rayleigh number and its critical value. Then the rate of exponential growth (for $\Delta R > 0$) or exponential decay (for $\Delta R < 0$) increases with the value of $|\Delta R|$.

We have now recapitulated the elementary linear theory. From now on we work exclusively with the square geometry for a single cell. Thereby we fix the preferred wave number to $k = \pi$. The amplitude ratio for the eigenfunctions is $B/A = 2\pi^2$ at marginal stability, according to eq. (17). The critical Rayleigh number for a square fluid-filled cavity is

$$R_c = R_{marginal}(\pi) = 8\pi^4 = 779.273, \tag{18}$$

according to eq. (16). the marginal Rayleigh number for the second horizontal onset mode with wave number $k = 2\pi$

$$R_{marginal}(2\pi) = \frac{125}{4}\pi^4 = 3044.034. \tag{19}$$

This is the second most unstable mode, which needs a Rayleigh number almost four times the critical value R_c in order to grow.

This paper distinguishes between two different routes for initiating transient nonlinear convection, with a fixed supercritical Rayleigh number. One route is the kickstart of the thermomechanical flow with a finite initial amplitude, to be considered below.

The other route is the more conventional soft start of nonlinear convection. This is the gradual evolution of the nonlinear flow from unstable perturbations. Then we consider an initial state with very small amplitude so that linear theory is valid during an early stage.

A. Unstable flow in a square according to linearized theory

We will now investigate the route of gradual evolution, by solving the general initial value problem according to linearized theory, with a given supercritical Rayleigh number $R > R_c$ for the square cavity filled with Newtonian fluid. From eq. (17) we find the relationship between the amplitude A of vertical velocity and the temperature amplitude B at marginal stability

$$\frac{B}{A} = 2\pi^2, \tag{20}$$

valid for a square cavity filled with fluid, where $k = 1$ for the lowest mode. So far, we have not introduced lateral boundary conditions, as we have only used the normal modes valid for an infinite horizontal domain. The only boundary conditions for cell walls that are compatible with normal modes are

$$\psi = \omega = \frac{\partial \theta}{\partial x} = 0, \text{ at } x = 0 \text{ and } x = 1. \tag{21}$$

These conditions represent impermeable, stress-free walls that are thermally insulating. They apply to our general nonlinear initial value problem, illustrated in Figure 1 above.

It is essential for our further analysis that the strict coupling ratio B/A according to eq. (20) between the amplitudes of velocity and temperature exists only at the critical Rayleigh number $R_c = 8\pi^4$, linked to the preferred onset mode for the square. With a supercritical Rayleigh number ($R > R_c$), no such coupling constraint B/A can be allowed. The transient problem is to be started with independent initial amplitudes $A(0)$ and $B(0)$ for temperature and vertical velocity, respectively. This is true both for the fully nonlinear transient problem and its linearized version, which we will completely solve before we attack the nonlinear evolution of convection.

In the general linearized analysis of the unstable (supercritical) flow, the amplitudes A for the temperature and B for the vertical velocity are initially independent. This means that the linearized transient problem consists of determining the functions $A(t)$ and $B(t)$ for the single Fourier mode for the temperature perturbation

$$\theta(x,y,t) = A(t)\cos(\pi x)\sin(\pi y), \tag{22}$$

and the associated vertical velocity

$$v(x,y,t) = B(t)\cos(\pi x)\sin(\pi y). \tag{23}$$

The exposition of the linearized normal-mode instability problem has led to the impression that the temperature perturbation $\theta(x,y,t)$ and the vertical velocity $v(x,y,t)$ are completely analogous and mathematically equivalent functions for solving the problem, differing only by a constant of proportionality in their respective amplitudes $A(t)$ and $B(t)$.

For solving the transient linearized problem we need the associated formulas for the streamfunction

$$\psi(x,y,t) = -\frac{1}{\pi}B(t)\sin(\pi x)\sin(\pi y), \tag{24}$$

and the vorticity

$$\omega(x,y,t) = -2\pi B(t)\sin(\pi x)\sin(\pi y). \tag{25}$$

From the linearized equations we derive the two coupled first-order differential equations for $A(t)$ and $B(t)$

$$\left(\frac{d}{dt} + 2\pi^2\right)A = B, \tag{26}$$

$$\left(Pr^{-1}\frac{d}{dt} + 2\pi^2\right)B = \frac{R}{2}A. \tag{27}$$

The functions $A(t)$ and $B(t)$ thus satisfy the same second-order equation,

$$\left(Pr^{-1}\frac{d^2}{dt^2} + 2\pi^2(Pr^{-1}+1)\frac{d}{dt} + \frac{R_c - R}{2}\right)A = 0, \tag{28}$$

$$\left(Pr^{-1}\frac{d^2}{dt^2} + 2\pi^2(Pr^{-1}+1)\frac{d}{dt} + \frac{R_c - R}{2}\right)B = 0, \tag{29}$$

where we have introduced $R_c = 8\pi^4$. The solutions can be written as

$$A(t) = A_1 e^{\sigma_1 t} + A_2 e^{\sigma_2 t}, \;\; B(t) = B_1 e^{\sigma_1 t} + B_2 e^{\sigma_2 t}. \tag{30}$$

There are two exponential rates σ given by the quadratic characteristic equation

$$\sigma^2 + 2\pi^2(1+Pr)\sigma - \frac{Pr\Delta R}{2} = 0. \tag{31}$$

These two rates of growth or decay are

$$\sigma_1 = \pi^2(1+Pr)\left(\sqrt{1 + \frac{Pr\Delta R}{2\pi^4(1+Pr)^2}} - 1\right). \tag{32}$$

$$\sigma_2 = -\pi^2(1+Pr)\left(\sqrt{1 + \frac{Pr\Delta R}{2\pi^4(1+Pr)^2}} + 1\right). \tag{33}$$

We have introduced $\Delta R = R - R_c = R - 8\pi^4$ for the difference between the given (supercritical) Rayleigh number and its critical value. Below will check whether oscillatory damping may happen for subcritical Rayleigh numbers, but there are no oscillations according to linearized supercritical theory, with $\Delta R > 0$. The single exponential growth rate $\sigma_1 > 0$ takes care of the instability, and there is an accompanying exponential decay rate $\sigma_2 < 0$. The solutions for the amplitudes are rewritten as

$$A(t) = A_1 e^{\sigma_1 t} + A_2 e^{\sigma_2 t}, \tag{34}$$

$$B(t) = (\sigma_1 + 2\pi^2)A_1 e^{\sigma_1 t} + (\sigma_2 + 2\pi^2)A_2 e^{\sigma_2 t}. \tag{35}$$

There are two independent initial conditions, represented indirectly by the two constants A_1 and A_2. We want to take as independent initial values the temperature amplitude A_0 and the vertical velocity amplitude B_0, defined as

$$A_0 = A(0), \;\; B_0 = B(0). \tag{36}$$

Then the parameters A_1 and A_2 are expressed in terms of A_0 and B_0. Insertion of $t = 0$ in the functions $A(t)$ and $B(t)$ gives $A_0 = A_1 + A_2$ and $B_0 = \sigma_1 A_1 + \sigma_2 A_2 + 2\pi^2 A_0$. The solutions of these equations are

$$A_1 = \frac{-(\sigma_2 + 2\pi^2)A_0 + B_0}{\sigma_1 - \sigma_2}, \tag{37}$$

$$A_2 = \frac{(\sigma_1 + 2\pi^2)A_0 - B_0}{\sigma_1 - \sigma_2}, \tag{38}$$

to be inserted in the solutions (34) - (35), giving

$$A(t) = \frac{\sigma_1 e^{\sigma_2 t} - \sigma_2 e^{\sigma_1 t}}{\sigma_1 - \sigma_2}A_0 + \frac{e^{\sigma_2 t} - e^{\sigma_1 t}}{\sigma_1 - \sigma_2}(2\pi^2 A_0 - B_0), \tag{39}$$

$$B(t) = \frac{(\sigma_1 + 2\pi^2)(\sigma_2 + 2\pi^2)}{\sigma_1 - \sigma_2}(e^{\sigma_2 t} - e^{\sigma_1 t})A_0 + \frac{(\sigma_1 + 2\pi^2)e^{\sigma_1 t} - (\sigma_2 + 2\pi^2)e^{\sigma_2 t}}{\sigma_1 - \sigma_2}B_0. \tag{40}$$

We have now established the general time evolution of the amplitudes $A(t)$ and $B(t)$ according to linearized theory. We have expressed the functions $\theta(x,y,t)$ and $v(x,y,t)$ in terms of their initial values $A(0) = A_0$ and $B(0) = B_0$.

A nonlinear initial value problem will face the broad challenge of systematics: How to choose generic initial conditions without too much bias. A background for handling these dilemmas is a good overview of the linearized evolution.

We will therefore consider four special cases where the linearized thermomechanical flow has some kind of synchronization. Firstly, the case where there is no initial flow, which means that the thermal mode triggers the entire convective

flow. Secondly, the case where there is no initial temperature perturbation, with the emerging temperature field owing its existence to the initial flow mode. The third case is the case of strict synchronization, where there is a pure exponential growth of the entire thermomechanical field. The fourth special case that we find important is the strict coupling of the amplitudes that exist at marginal stability. We want to see how this coupling is being loosened for a transient supercritical flow.

B. On subcritical damping and possible oscillations

The exponential decay when $R < R_c$ will take place only if the square root in the formulas (32) - (33) has a non-negative argument. Introducing $\Delta R = R - R_c = R - 8\pi^4$, we see that the necessary condition for oscillatory behavior of the perturbations is

$$\frac{R}{8\pi^4} < -\frac{(1-Pr)^2}{4Pr}, \tag{41}$$

showing that oscillations for the linearized problem require a negative Rayleigh number. These oscillations are expected to represent Brunt-Väisälä frequencies of stable stratification[6], but such wave phenomena are not covered by the present theory. Yet eq. (41) shows that the special value $Pr = 1$ is the only case where all negative Rayleigh numbers give oscillations. For any Prandtl number different from one, there will be a domain of negative Rayleigh numbers where the disturbances will decay exponentially without oscillations. Therefore, one may suspect that $Pr = 1$ is the value where the strongest nonlinear transient oscillations may be triggered, which seems plausible according to our numerical simulations below.

The special case of $Pr = 1$ and $R = 0$ has only one damping rate of the lowest thermomechanical modes (22) - (23), which is $\sigma_1 = \sigma_2 = -2\pi^2$. The innocent-looking thermal disturbances $\sin(n\pi y)$, with no x dependence and without any associated flow field, will then include a mode $n = 1$ with the slowest possible damping. These modes decay in time as follows

$$\theta = \theta_0\, e^{-n^2\pi^2 t} \sin(n\pi y), \tag{42}$$

with θ_0 denoting the initial amplitude. This decay does not depend on R or Pr, so it is always the same, governed by the heat diffusion equation without a convection term. This type of initial disturbance does not influence the linearized onset problem, but it may become significant for the kick-started convection that we will study by a small-time expansion below. We disregard such purely thermal modes (with no influence on the linear stability problem) in the present work, noting their possible significance through their ability to disturb the delicate symmetries, as discussed in the Appendix.

C. Initiating the linearized convection from rest

We consider the special case where the flow starts from rest, so that $B_0 = B(0) = 0$. Then the initial temperature amplitude $A(0)$ remains as the only nonzero amplitude, leading to the solutions

$$A(t) = \frac{(\sigma_1 + 2\pi^2)e^{\sigma_2 t} - (\sigma_2 + 2\pi^2)e^{\sigma_1 t}}{\sigma_1 - \sigma_2} A_0, \tag{43}$$

$$B(t) = \frac{(\sigma_1 + 2\pi^2)(\sigma_2 + 2\pi^2)}{\sigma_1 - \sigma_2} (e^{\sigma_2 t} - e^{\sigma_1 t}) A_0, \tag{44}$$

reduced from the general formulas (39) and (40).

D. Linearized flow initiation without an initial thermal field

We will consider the case where there is an initial flow field with zero temperature perturbation. This means that $A_0 = A(0) = 0$, with the initial amplitude $B(0)$ of the vertical velocity as the only nonzero amplitude. The solutions are

$$A(t) = \frac{e^{\sigma_1 t} - e^{\sigma_2 t}}{\sigma_1 - \sigma_2} B_0, \tag{45}$$

$$B(t) = \frac{(\sigma_1 + 2\pi^2)e^{\sigma_1 t} - (\sigma_2 + 2\pi^2)e^{\sigma_2 t}}{\sigma_1 - \sigma_2} B_0. \tag{46}$$

It is interesting to compare the structure of these solutions for $A(t)$ and $B(t)$ with the corresponding formulas (43) - (44). We thus compare cases where only one instability mechanism is active initially since the other perturbation needed for instability is initially inactive with zero amplitude. Nevertheless, the supercritical growth of instabilities is able to revive the other mode starting from zero. This is not possible at marginal stability, again confirming that the amplitudes $A(0)$ and $B(0)$ cannot be independent at marginal stability. Eq. (45) shows how the thermal mode is started from zero aided by the flow mode of instability. It can be directly compared with eq. (44), which shows how the flow mode is started from zero aided by the thermal mode of instability.

The differences in these solutions reveal asymmetries in the roles of buoyancy and convective transport for the linear stability theory of convection. These asymmetries will escalate once nonlinearity gains importance.

E. The initiation that gives exponential growth according to linear theory

One may prefer to start the nonlinear process as a purely exponential growth during the early stage when linear theory is valid. This type of evolution takes place when $A_2 = 0$, to be combined with the induced relationship $B_0 = (\sigma_1 + 2\pi^2)A_0$. The initial temperature amplitude $A(0) = A_0$ is arbitrary in linear theory, while the initial velocity amplitude $B(0) = B_0$ must be chosen according to the rewritten relationship

$$\frac{B_0}{A_0} = \sigma_1 + 2\pi^2 = \pi^2(1-Pr) + \pi^2(1+Pr)\sqrt{1 + \frac{Pr\Delta R}{2\pi^4(1+Pr)^2}}. \tag{47}$$

after inserting the formula (32) for the growth rate σ_1. Making this choice of linking B_0 to the initial temperature amplitude A_0, so that $A_2 = 0$, eliminates the decay rate σ_2 from the entire time evolution. Linear theory prescribes a very simple growth process

$$A(t) = A_0 e^{\sigma_1 t}, \;\; B(t) = B_0 e^{\sigma_1 t}, \tag{48}$$

which implies that the ratio $B(t)/A(t) = B_0/A_0 = \sigma_1 + 2\pi^2$ remains constant as long as linear theory is valid. A more complicated behavior will gradually emerge as the nonlinear terms in the governing equations accumulate large-amplitude dominance over the linearized terms responsible for the early exponential growth. In Figure 5 below, we will extract the ratio $A(t)/B(t)$ for initial value problems with very small amplitudes with fully nonlinear simulations. Linear theory is valid as long as the ratio $B(t)/A(t)$ remains constant.

F. Maintaining initially the coupling at marginal stability

We will now study the transient evolution under the strict coupling (20). It exists only at marginal stability since the initial value problem of finite-amplitude convection allows the initial amplitudes $A(0) = A_0$ and $B(0) = B_0$ to be chosen independently. We will now study the special case

$$\frac{B_0}{A_0} = 2\pi^2, \tag{49}$$

where we maintain the amplitude coupling at marginal stability. This situation can be mimicked experimentally by a gradually increased Rayleigh number beyond the critical value, with random perturbations from which the unstable ones will be naturally selected to start with this given amplitude ratio (20).

The general solution (39)-(40) with the constraint (20) will reduce to

$$A(t) = A_0 \frac{(\sigma_1 + 2\pi^2)e^{\sigma_2 t} - \sigma_2 e^{\sigma_1 t}}{\sigma_1 - \sigma_2}, \tag{50}$$

$$B(t) = A_0 \frac{(\sigma_1 + 2\pi^2)\sigma_2 e^{\sigma_2 t} - (\sigma_2 + 2\pi^2)\sigma_1 e^{\sigma_1 t}}{\sigma_1 - \sigma_2}. \tag{51}$$

After an initial stage where the decay rate σ_2 plays a role, the later process is totally dominated by the exponential growth rate σ_1, where the evolution of the amplitudes have the approximate evolution

$$A(t) = -A_0 \sigma_2 \frac{e^{\sigma_1 t}}{\sigma_1 - \sigma_2}, \tag{52}$$

$$B(t) = -A_0 \sigma_1 \frac{(\sigma_2 + 2\pi^2)e^{\sigma_1 t}}{\sigma_1 - \sigma_2}, \tag{53}$$

whereby the ratio $B(t)/A(t)$ again approaches a constant value for large values of t

$$\frac{B(t)}{A(t)} \to \sigma_1 \left(1 - \frac{2\pi^2}{|\sigma_2|}\right), \tag{54}$$

where the absolute value sign serves as a reminder that σ_2 is negative. However, this asymptotic version of the linearized growth process is not representative once the nonlinear terms gain importance. We include it to demonstrate that the ratio $B(t)/A(t)$ evolves away from its initial value B_0/A_0. The role of the Prandtl number indicates why the initial value of the ratio (20) is efficiently wiped out and does not reappear in the later transient process, according to linear theory. While the marginal state is independent of the Prandtl number, any unstable supercritical state depends on the Prandtl number through the growth rate σ_1.

G. On slowly initiated transient nonlinear convection

We have now investigated the linearized first stage of a gradual route to transient nonlinear convection. This gives a natural approach to supercritical convection, which can be followed up experimentally by heating a fluid layer slowly from below. With a controlled experiment allowing only small disturbances, the heating of the fluid layer can be stopped at a finite supercritical Rayleigh number before the unstable flow has reached an amplitude where nonlinear effects become important. The preferred modes of disturbance for the temperature and vertical velocity can then gradually grow into finite amplitude thermomechanical flow, as prescribed in the above analytical theory as far as the early linearized stage is concerned. However, the set of preferred modes at marginal stability do not have independent initial amplitudes, as they may emerge only with a fixed amplitude ratio.

The relative magnitude of a pair of small-amplitude modes will usually change during their initial stage of exponential growth before nonlinearity becomes important. It is therefore of limited interest to select two independent small initial amplitudes for a supercritical flow.

In the next section, we will pursue analytically a physically richer and complementary route of kick-starting the nonlinear transient flow. Here we initiate the flow at $t = 0$ with two independent normal modes for the temperature perturbation and the flow field. The respective initial amplitudes A_0 and B_0 for temperature and flow will be chosen to be large, in contrast to the small initial amplitudes we have been considering in the linearized theory. These large-amplitude modes will immediately perform strong nonlinear interactions, evolving with time.

The disadvantage with kick-starting the nonlinear process is that it is difficult to represent experimentally. The obvious advantage of kick-starting nonlinearity is that it can be modeled analytically and used for benchmarking our numerical methods and tools.

IV. ON KICK-STARTED TRANSIENT NONLINEAR CONVECTION

We will now investigate the initial value problem with large initial amplitude. As a general initial condition, we take the combination of one single normal mode for the temperature

perturbation and one single normal mode for the vertical velocity. Albeit only initially, these modes will have independent finite amplitudes, thereby kick-starting the strongly coupled nonlinear process already at small dimensionless times.

A. An asymptotic small-time expansion

As initial condition we take the pair of normal modes

$$\theta(x,y,0) = A\cos(\pi x)\sin(\pi y), \;\; v(x,y,0) = B\cos(\pi x)\sin(\pi y), \tag{55}$$

representing the preferred onset modes at marginal stability, but the Rayleigh number R is now assumed to have a supercritical value $R > R_c = 8\pi^4$ for the square geometry. A kick-start of nonlinear convection with amplitudes A and B requires that $A \gg A_0$ or $B \gg B_0$. Here A_0 and B_0 are the legal amplitudes (36) according to linearized theory.

The reason that we choose the initial distribution of the vertical velocity as the flow variable associated with an initial amplitude B, is that it has the same mathematical form as the temperature perturbation, which takes care of the other initial amplitude A. These interesting parallels in flow and temperature initiations would be lost if we had chosen the initial amplitude of the streamfunction (or the vorticity) as the second independent initial condition. In the linear theory of marginal stability, we already found that the velocity amplitude B is much greater than the temperature amplitude, see eq. (20). This amplitude difference in favor of the flow will prevail in nonlinear theory, and the underlying reason is that the standard dimensionless equations (2) - (3) does not scale the velocity with respect to buoyancy, which would be a correct physical scaling. The temperature is scaled correctly, but the lack of dimensionless parameters in the heat equation (3) scales the velocity with the thermal variables alone. Mathematically, this standard description is formally correct. However, the physical comparison of flow amplitude and thermal amplitude is blurred when a balanced physical scaling is lacking.

The early evolution of a kick-started initial state can be expressed by the small-time expansion

$$\psi(x,y,t) = \psi_0(x,y) + t\,\psi_1(x,y)) + t^2\psi_2(x,y) + .., \tag{56}$$

$$\omega(x,y,t) = \omega_0(x,y) + t\,\omega_1(x,y) + t^2\omega_2(x,y) + .., \tag{57}$$

$$\theta(x,y,t) = \theta_0(x,y) + t\,\theta_1(x.y) + t^2\theta_2(x,y) + ... \tag{58}$$

We recall that at each order n we have the identity $\omega_n = -\nabla^2\psi_n$. Inserting these series into the nonlinear equations (8) and (9) and take the limit $t \to 0$ gives the equations for the first-order vorticity

$$\omega_1 = -\frac{\partial\psi_0}{\partial y}\frac{\partial\omega_0}{\partial x} + \frac{\partial\psi_0}{\partial x}\frac{\partial\omega_0}{\partial y} + PrR\frac{\partial\theta_0}{\partial x} + Pr\nabla^2\omega_0, \tag{59}$$

and the first-order temperature

$$\theta_1 = -\frac{\partial\psi_0}{\partial x} - \frac{\partial\psi_0}{\partial y}\frac{\partial\theta_0}{\partial x} + \frac{\partial\psi_0}{\partial x}\frac{\partial\theta_0}{\partial y} + \nabla^2\theta_0. \tag{60}$$

The second-order vorticity ω_2 and the second-order temperature θ_2 are found in a similar way. We first differentiate the full nonlinear equations in time, leading to the equations

$$2\omega_2 = -\frac{\partial\psi_1}{\partial y}\frac{\partial\omega_0}{\partial x} - \frac{\partial\psi_0}{\partial y}\frac{\partial\omega_1}{\partial x} + \frac{\partial\psi_1}{\partial x}\frac{\partial\omega_0}{\partial y} + \frac{\partial\psi_0}{\partial x}\frac{\partial\omega_1}{\partial y} + PrR\frac{\partial\theta_1}{\partial x} + Pr\nabla^2\omega_1, \tag{61}$$

$$2\theta_2 = -\frac{\partial\psi_1}{\partial x} - \frac{\partial\psi_1}{\partial y}\frac{\partial\theta_0}{\partial x} - \frac{\partial\psi_0}{\partial y}\frac{\partial\theta_1}{\partial x} + \frac{\partial\psi_1}{\partial x}\frac{\partial\theta_0}{\partial y} + \frac{\partial\psi_0}{\partial x}\frac{\partial\theta_1}{\partial y} + \nabla^2\theta_1. \tag{62}$$

Below we will also include nonlinear elements of the third and fourth-order solutions, which are terms with amplitudes A^mB^n where the sum $m+n \geq 2$. Terms with amplitudes A^1B^0 and A^0B^1 are not in themselves interesting for describing the kick-start since they are already included in the general linear theory given above. Yet, we need to include all these terms of first power in the amplitude to the first two orders in time in order to include all higher-order nonlinear terms.

B. Solutions to zeroth and first order for the kick-start

We have chosen the zeroth-order solution (55) for the kick-start, to be reformulated as

$$\theta_0 = A\cos(\pi x)\sin(\pi y), \;\; \psi_0 = -\frac{B}{\pi}\sin(\pi x)\sin(\pi y),$$
$$\omega_0 = -2\pi B\sin(\pi x)\sin(\pi y). \tag{63}$$

It is now used to calculate the exact first-order solution, which is found to be

$$\theta_1 = (B - 2\pi^2 A)\cos(\pi x)\sin(\pi y) - \frac{\pi}{2}AB\sin(2\pi y), \tag{64}$$

$$\psi_1 = Pr\left(2\pi B - \frac{R}{2\pi}A\right)\sin(\pi x)\sin(\pi y), \tag{65}$$

$$\omega_1 = \pi Pr\left(4\pi^2 B - RA\right)\sin(\pi x)\sin(\pi y). \tag{66}$$

The first term in the formula (64) for θ_1 is given by linear theory. We note the sign of its amplitude $(B - 2\pi^2 A)$, as it is known from eq. (20) to be zero at marginal stability. This initial temperature mode $\cos(\pi x)\sin(\pi y)$ will therefore start increasing for small times when $B > 2\pi^2 A$, while it starts decreasing when $B < 2\pi^2 A$. Below we will study how different choices of A and B provide a variation in the behavior during the early stages of supercritical convection.

The only nonlinear term (with the amplitude product AB) is the second harmonic vertical temperature field independent of x, accounting for the early convective heat transfer. Its amplitude is proportional to the products of the initial flow amplitude and the initial temperature amplitude. This shows that

even if these amplitudes are independent in the nonlinear initial value problem, both of them need to be given finite values for the process to become nonlinear during a dimensionless time unit.

The thermal field $\sin(2\pi y)$ with the quadratic amplitude AB could have been included already in the zeroth-order solution for the kick-start. It is a member $n = 2$ of the family of thermal eigenfunctions (42), which will always decay and do not affect the linearized stability criterion. In the kick-start approach to nonlinear convection, they may, in principle, become important. These zero wave number thermal modes are neglected, in order to maintain the strict single mode initiation of the present model. If such solutions had been added, they would have enhanced the vortex interactions by allowing them to emerge at lower orders in the small-time expansion. Moreover, the odd numbers n for the thermal modes $\sin(n\pi y)$ would abolish the present strict symmetry/antisymmetry restrictions, which we elaborate on in Appendix A.

C. The full second-order solution for the kick-start

The second-order temperature field is composed of three Fourier components

$$\theta_2 = a_{11}\cos(\pi x)\sin(\pi y) + a_{13}\cos(\pi x)\sin(3\pi y) + a_{02}\sin(2\pi y). \tag{67}$$

Each of the three coefficients contains nonlinear terms in the initial amplitudes A and B.

$$a_{11} = \left(2\pi^4 + \frac{PrR}{4}\right)A - \pi^2(1+Pr)B - \frac{\pi^2}{4}AB^2, \tag{68}$$

$$a_{13} = \frac{\pi^2}{4}AB^2, \tag{69}$$

$$a_{02} = -\frac{\pi}{8}PrRA^2 - \frac{\pi}{4}B^2 + \frac{\pi^3}{2}(3+Pr)AB. \tag{70}$$

The second-order solution for the vorticity still contains only linearized terms

$$\omega_2 = \pi Pr\left(\pi^2 R(1+Pr)A - \frac{R}{2}B - 4\pi^4 PrB\right)\sin(\pi x)\sin(\pi y), \tag{71}$$

with the underlying streamfunction

$$\psi_2 = \frac{Pr}{2\pi}\left(\pi^2 R(1+Pr)A - \frac{R}{2}B - 4\pi^4 PrB\right)\sin(\pi x)\sin(\pi y). \tag{72}$$

D. Nonlinear flow effects in the third-order solution

We will now only include nonlinear velocity contributions in the third-order solution. Already the second-order temperature includes the triple amplitude products AB^2, in contrast to the lacking nonlinear terms for the flow. It is important to see how nonlinearity for the flow is triggered when there is only one mode of instability represented in the early nonlinear flow.

The third-order vorticity contains one notable term originating from the buoyancy term, which we introduce by writing the second derivative of the vorticity equation as

$$\frac{\partial^3\omega}{\partial t^3} = PrR\frac{\partial^3\theta}{\partial x\partial^2 t} + O(A^1, B^1), \tag{73}$$

where we insert the small-time expansion to get the third-order vorticity

$$\omega_3 = \frac{1}{3}PrR\frac{\partial\theta_2}{\partial x} + O(A^1, B^1). \tag{74}$$

Even though this third-order buoyancy term is a formally linear term in the vorticity equation, its origin is from the lower-order (second) nonlinear convection term contributing to the second-order temperature, which we see by inserting from eq. (67), giving

$$\omega_3 = PrR\frac{\pi^3}{12}AB^2\sin(\pi x)(\sin(\pi y) - \sin(3\pi y)) + O(A^1, B^1), \tag{75}$$

with the underlying streamfunction

$$\psi_3 = PrR\frac{\pi}{24}AB^2\sin(\pi x)\left(\sin(\pi y) - \frac{1}{5}\sin(3\pi y)\right) + O(A^1, B^1). \tag{76}$$

Here the first higher Fourier mode $\sin(3\pi y)$ emerges for the flow, to third order in time. Its amplitude is proportional to A^1, the first power of the initial temperature amplitude. and to the second order of the initial flow amplitude. Still there are no vortex interactions, since this nonlinear effect was imported to the vorticity equation through the linear buoyancy term. We must go to fourth order in time in order to find the first nonlinear vortex interaction.

We note the role of the Prandtl number for this third-order nonlinear flow effects. A low Prandtl number does not stimulate but rather impede the slowly emerging nonlinearity. This is because there are no vortex interactions early stages of evolution from a single-mode initial thermomechanical state. The unit Prandtl number will be chosen in our simulations below, since $Pr = 1$ represents a compromise in overcoming obstacles for the initiating vortex interactions as well as obstacles for their escalations after they have been started.

E. Nonlinear vortex interactions in the fourth-order solution

It is only the Fourier term $\sin(\pi x)\sin(3\pi y)$ in the third-order flow that contributes to the vorticity generation to fourth order, which is actually the leading-order vorticity interaction according to the small-time expansion. From an analytical point of view, it is an open question whether this fourth-order interaction will be significant at all. This is because the small-time expansion is an asymptotic series that breaks down quite suddenly when four terms are included, and there is at best a very short time interval available for fourth-order effects to

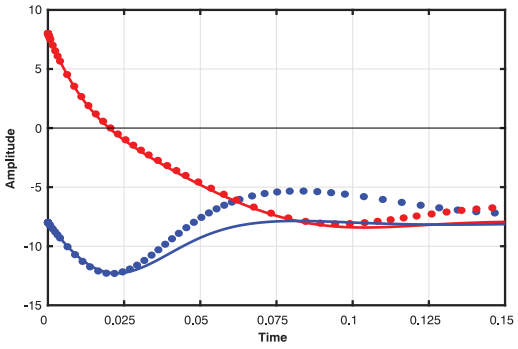

FIG. 2. The evolution of the leading Fourier amplitude for the streamfunction, with two examples of kick-start for a moderately supercritical Rayleigh number. Both the flow and the temperature start with nonzero amplitudes. The solid curves show numerical simulations for the evolution of $\psi(0.5,0.5,t)$ with $R = 4R_c = 32\pi^4$ and $Pr = 1$.
Lower curve: $\theta(x,y,0) = \cos(\pi x)\sin(\pi y$, $\psi(x,y,0) = -8\sin(\pi x)\sin(\pi y)$, $\omega(x,y,0) = 16\pi^2\sin(\pi x)\sin(\pi y)$.
Upper curve: $\theta(x,y,0) = \cos(\pi x)\sin(\pi y$, $\psi(x,y,0) = 8\sin(\pi x)\sin(\pi y)$, $\omega(x,y,0) = 16\pi^2\sin(\pi x)\sin(\pi y)$.
Two dotted graphs are added, representing the approximate evolution according to our Lorenz-type set of equations (82) - (86).

have influence before the series diverges and no longer represents the finite-amplitude interactions.

The fourth-order vorticity is derived from the third derivative of the vorticity equation, and can be expressed as

$$4\omega_4 = -\frac{\partial\psi_3}{\partial y}\frac{\partial\omega_0}{\partial x} - \frac{\partial\psi_0}{\partial y}\frac{\partial\omega_3}{\partial x} + \frac{\partial\psi_3}{\partial x}\frac{\partial\omega_0}{\partial y} + \frac{\partial\psi_0}{\partial x}\frac{\partial\omega_3}{\partial y} + O(B^2) \tag{77}$$

where we omit terms that do not represent vortex interactions. Formally this is done by excluding terms that do not contain the third power of the initial flow amplitude B. The formula for the fourth-order vorticity is

$$\omega_4 = \frac{\pi^4}{120}AB^3PrR\sin(2\pi x)(\sin(4\pi y) - 2\sin(2\pi y)) + O(B^2). \tag{78}$$

The corresponding streamfunction is

$$\psi_4 = \frac{\pi^2}{4800}AB^3PrR\sin(2\pi x)(2\sin(4\pi y) - 5\sin(2\pi y)) + O(B^2). \tag{79}$$

This fourth-order flow has a fourth-power dependency of the two initial amplitudes A and B. It is more strongly dependent on the flow amplitude (by the third-power term B^3) than the temperature amplitude (by the term A^1). Yet we see that both initial amplitudes A and B need to be nonzero in order to obtain vortex interactions.

The role of the Prandtl number is the same in this selected fourth-order vortex interaction term as we saw in the third-order terms (75) that we commented above. We note the second harmonic term $\sin(2\pi x)$ emerging from these leading-order vortex interactions in the horizontal direction. It contrasts all lower order solutions for the flow, which contain only the basic term $\sin(\pi x)$ introduced in the initial condition.

V. A LORENZ-TYPE SET OF COUPLED EQUATIONS

The small-time expansion is consistent for the early stages of kick-started nonlinear convection, but its small radius of convergence does not represent any oscillatory behavior. In order to capture analytically the full nonlinear time-dependence, we need to compromise somewhat on the exactness. The richest analytical model that we find feasible is a truncated set of five Fourier components

$$\begin{aligned}\theta(x,y,t) &= T_0(t)\sin(2\pi y)\\ &+T_1(t)\cos(\pi x)\sin(\pi y) + T_2(t)\cos(\pi x)\sin(3\pi y),\end{aligned} \tag{80}$$

$$\psi(x,y,t) = X_1(t)\sin(\pi x)\sin(\pi y) + X_2(t)\sin(\pi x)\sin(3\pi y). \tag{81}$$

This truncation is motivated from the small-time expansion, and is based on the assumption that nonlinear vortex interactions can be neglected. This means that buoyancy must have an early domination over inertial forces, otherwise a reversal of rotation cannot take place during the transient motion. In the manner of the Lorenz equations[24], we will therefore derive five coupled equations for the time derivatives of the five amplitudes derived above.

The inserting of truncated solutions into the nonlinear equations is perform in a manner where we neglect the interaction terms that do not belong to these five Fourier terms. There are no self-interactions from the two normal-mode vortices. There are only linearized terms contributing to the vorticity equation (8), with two evolution equations emerging

$$\frac{dX_1}{dt} = -2\pi^2 PrX_1 - \frac{Pr}{2\pi}RT_1, \tag{82}$$

$$\frac{dX_2}{dt} = -10\pi^2 PrX_2 - \frac{Pr}{10\pi}RT_2. \tag{83}$$

The three evolution equations resulting from inserting the truncated solutions into the heat equation (9) are all nonlinear, and are listed here

$$\frac{dT_0}{dt} = -4\pi^2 T_0 + \frac{\pi^2}{2}X_1T_1 - \frac{\pi^2}{2}X_2T_1 - \frac{\pi^2}{2}X_1T_2, \tag{84}$$

$$\frac{dT_1}{dt} = -2\pi^2 T_1 - \pi X_1 - \pi^2 X_1T_0 + \pi^2 X_2T_0, \tag{85}$$

$$\frac{dT_2}{dt} = -10\pi^2 T_2 - \pi X_2 + \pi^2 X_1T_0. \tag{86}$$

The lowest thermal Fourier mode excluded from these equations due to truncation is $\cos(2\pi x)\sin(2\pi y)$. The lowest excluded Fourier mode for the streamfunction is

$\sin(2\pi x)\sin(2\pi y)$. The same terms are the first ones to emerge in the small-time expansion without being included in our Lorenz-type equations.

This Lorenz-type set of equations is of fifth order in time, and has in total six quadratic coupling terms, in addition to its nine linear terms. It is natural to compare it with the original Lorenz set of equations[24]. The Lorenz set is of third order in time, and has only two quadratic coupling terms in addition to its five linear terms. We will not attempt a thorough discussion of our Lorenz-type system, but use it for one specific purpose.

Our aim is to describe flow reversals that we will encounter in our numerical simulations of the full nonlinear system. For maintaining consistency with our general model, three out of the five initial values must be put equal to zero, for the Fourier components that do not belong to the preferred onset modes. For our Lorenz-type system (82) - (86) we must then put

$$T_0(0) = T_2(0) = X_2(0) = 0. \tag{87}$$

Only the two initial amplitudes $T_1(0)$ and $X_1(0)$ remain to be chosen, as the appropriate independent parameters for our second-order initial value problem.

Figure 2 above shows computations for the Lorenz-type of five coupled equations (dotted graphs) together with numerical simulations of the full nonlinear initial value problem, for a Rayleigh number that is four times the critical value for the square. Only the leading streamfunction amplitude $X_1(t)$ is plotted, since it represents the magnitude and direction of the dominating spin inside the square. The compromised convergence of the truncated Lorenz-type set is exposed, since the solution starts to diverge after the first extremal value for the streamfunction amplitude.

The lower set of curves represents the case where the initial spin and the initial buoyancy torque has the same directions. In this case the spin will naturally maintain its initial direction.

The upper set of curves represents the case where the initial spin and the initial buoyancy torque are given opposite directions. This conflict will lead to one reversal of flow direction, where the initial buoyancy is able to overrule the initial spin and switch its direction. The case displayed in Figure 2 has only one flow reversal. We realized that the truncated Lorenz-type of equations do not have sufficient accuracy for capturing the set of several spin reversals that may occur at higher supercritical Rayleigh numbers. The Lorenz-type set of equation gives satisfactory convergence until the single reversal of flow direction is completed, for moderately supercritical Rayleigh numbers represented by Figure 2 where $R = 4R_c$.

VI. NUMERICAL SIMULATIONS WITH KICK-START

After these preliminary computations for testing the accuracy of the Lorenz-type set of ordinary differential equations, we will now present simulations of the full nonlinear problem for higher Rayleigh numbers.

The small-time expansion that we have carried out has produced Fourier terms of the type $\cos(m\pi x)\sin(n\pi y)$ for the temperature and terms of the type $\sin(m\pi x)\sin(n\pi y)$ for the streamfunction. A striking fact is that the sum $m+n$ is an even number for all these terms that we have calculated. In the Appendix, we show that this constraint is valid for all finite amplitude solutions, with our choice of initial conditions. We also show that it gives a temperature field that is antisymmetric around the mid-point of the square, while the flow field is symmetric.

Now we will show numerical simulations of the full nonlinear process, where we bear in mind the symmetry constraints demonstrated in the Appendix. We performed some preliminary numerical simulations with very small initial amplitudes, giving early stages of exponential growth. Only Figure 5 will display such results.

Some examples of kick-started moderately supercritical convection are shown in Figure 3. It shows the evolution of the streamfunction in the mid-point of the square $(0.5, 0.5)$ for a Rayleigh number that is twice the critical value $8\pi^4$, with $Pr = 1$. For this moderately supercritical Rayleigh number, the flow field has one totally dominating Fourier mode, which is the initial mode. This means that $\psi(0.5, 0.5, t)$ is practically equal to $-B_{11}(t)$. In Figure 3 we show three different combinations of initial values. The upper curve represents an initial temperature field with zero initial flow. The middle curve represents an initial flow field with zero initial temperature perturbation. The lower curve takes the previously chosen conditions and combines their nonzero initial values. The evolution for the third case is not a superposition of the two first cases because of the nonlinearity of the process. The dashed line is included as a superposition of the two independently started nonlinear solutions, just to illustrate how far this nonlinear process is away from obeying the principle of superposition. We note that the final steady state is the same for all three cases of initiation, depending only on the Rayleigh number and not on the initial amplitudes.

A. Spectral analysis for temperature and flow

For making a detailed comparison of the numerical simulations with the analytical formulas, we need to develop a spectral analysis for the numerical results. The total solution for the temperature perturbation is the double Fourier series

$$\theta(x,y,t) = \sum_{m=0}^{\infty}\sum_{n=1}^{\infty} A_{mn}(t)\cos(m\pi x)\sin(n\pi y), \tag{88}$$

which is coupled to the Fourier series for the vertical velocity

$$v(x,y,t) = \sum_{m=1}^{\infty}\sum_{n=1}^{\infty} B_{mn}(t)\cos(m\pi x)\sin(n\pi y), \tag{89}$$

These two Fourier series have the same form, with the single exception that the temperature perturbation contains terms independent of x. These terms are important, since they are responsible for the heat flux through the fluid layer. Above we have identified these Fourier terms independent of y as legal eigenfunctions for the linearized stability for $\theta(x,y,t)$, while they are illegal as eigenfunctions for the vertical velocity $v(x,y,t)$.

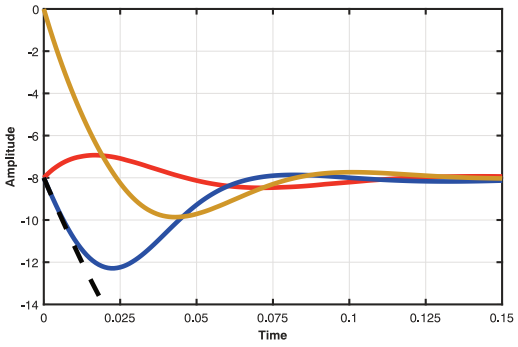

FIG. 3. The evolution of the leading Fourier amplitude for the streamfunction, with three different types of kick-start for a moderately supercritical Rayleigh number. A purely thermal initiation, a purely hydrodynamic initation, and the full thermomechanical combination of these two. We show the evolution of $\psi(0.5,0.5,t)$ with different initial conditions for $R = 4R_c = 32\pi^4$ and $Pr = 1$.
Yellow (upper) curve: $\theta(x,y,0) = \cos(\pi x)\sin(\pi y)$, $\psi(x,y,0) = 0$, $\omega(x,y,0) = 0$.
Red (middle) curve: $\theta(x,y,0) = 0$, $\psi(x,y,0) = -8\sin(\pi x)\sin(\pi y)$, $\omega(x,y,0) = -16\pi^2\sin(\pi x)\sin(\pi y)$.
Blue (lower) curve: $\theta(x,y,0) = \cos(\pi x)\sin(\pi y)$, $\psi(x,y,0) = -8\sin(\pi x)\sin(\pi y)$, $\omega(x,y,0) = -16\pi^2\sin(\pi x)\sin(\pi y)$.
Additional (dashed) black curve: This is a fictitious solution obtained by superposing the solutions represented by yellow and blue curves.

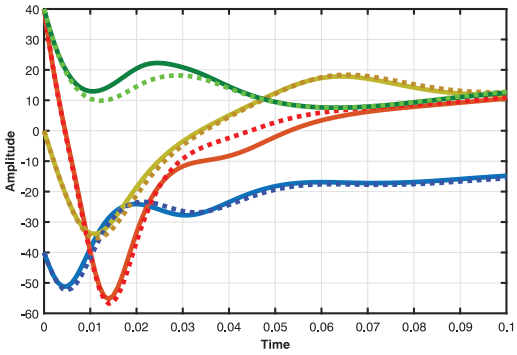

FIG. 4. The evolution of the streamfunction amplitude in the mid-point of the square is displayed for initiations similar to Figure 3, with twice as large Rayleigh number. We also show how the full solution differs from the amplitude evolution of the leading Fourier mode. The solid curves show the evolution of $\psi(0.5,0.5,t)$ with different initial conditions for $R = 8R_c = 64\pi^4$ and $Pr = 1$. Dotted lines are added, representing the spectral component $-B_{11}(t)/\pi$. The different graphs can be identified by their initial amplitudes.
Yellow curves (intermediate) show purely thermal initiation: $\theta(x,y,0) = 5\cos(\pi x)\sin(\pi y)$, $\psi(x,y,0) = 0$, $\omega(x,y,0) = 0$.
Blue (lower) curves show purely : $\theta(x,y,0) = 5\cos(\pi x)\sin(\pi y)$, $\psi(x,y,0) = -40\sin(\pi x)\sin(\pi y)$, $\omega(x,y,0) = -80\pi^2\sin(\pi x)\sin(\pi y)$.
Green (upper) curves: $\theta(x,y,0) = 5\cos(\pi x)\sin(\pi y)$, $\psi(x,y,0) = 40\sin(\pi x)\sin(\pi y)$, $\omega(x,y,0) = 80\pi^2\sin(\pi x)\sin(\pi y)$.
Red curves (with greatest variations): $\theta(x,y,0) = 10\cos(\pi x)\sin(\pi y)$, $\psi(x,y,0) = 40\sin(\pi x)\sin(\pi y)$, $\omega(x,y,0) = 80\pi^2\sin(\pi x)\sin(\pi y)$.

From the definition $v = -\partial\psi/\partial x$ we derive the Fourier series for the streamfunction

$$\psi(x,y,t) = \sum_{m=1}^{\infty}\sum_{n=1}^{\infty} C_{mn}(t)\sin(m\pi x)\sin(n\pi y), \qquad (90)$$

where the new coefficients obey the relationship $-m\pi C_{mn} = B_{mn}$ so they can be replaced by those for the vertical velocity

$$\psi(x,y,t) = -\frac{1}{\pi}\sum_{m=1}^{\infty}\sum_{n=1}^{\infty}\frac{B_{mn}(t)}{m}\sin(m\pi x)\sin(n\pi y). \qquad (91)$$

The vorticity field is $\omega = -\nabla^2\psi$

$$\omega(x,y,t) = -\pi\sum_{m=1}^{\infty}\sum_{n=1}^{\infty}\frac{m^2+n^2}{m}B_{mn}(t)\sin(m\pi x)\sin(n\pi y). \qquad (92)$$

The spectral decomposition of the numerical results for the temperature field is based on the integral

$$\int_0^1\int_0^1 \theta(x,y,t)\cos(i\pi x)\sin(j\pi y)dxdy = \frac{A_{ij}(t)}{4}, \text{ when } i > 0, \qquad (93)$$

to be supplemented with the exceptional case $i = 0$ where this integral has the value $A_{0j}/2$. Hereby the set of Fourier coefficients can be extracted from the numerical results. A spectral analysis for the vertical velocity applies the similar formula

$$B_{ij}(t) = 4\int_0^1\int_0^1 v(x,y,t)\cos(i\pi x)\sin(j\pi y)dxdy, \text{ when } i > 0, \qquad (94)$$

with the difference that there are no terms with $i = 0$. Since we work with the streamfunction ψ, we can alternatively write

$$C_{ij}(t) = 4\int_0^1\int_0^1 \psi(x,y,t)\sin(i\pi x)\sin(j\pi y)dxdy, \qquad (95)$$

where the Fourier coefficients C_{ij} for the streamfunction are given by $v = -\partial\psi/\partial x$. These coefficients are linked to those for the vertical velocity as follows: $B_{ij} = -i\pi C_{ij}$, where i and j are positive integers.

1. *Numerical results for spectral components*

Figure 4 is analogous to Figure 3 , with similar initial conditions for twice as high Rayleigh number $R = 64\pi^4$. The solid lines represent the evolution of the streamfunction evaluated in the mid-point, adding a dotted line representing the amplitude of the leading mode. These two curves would be identical if the onset mode of motion was alone, so the deviation represent the importance of higher Fourier modes for the motion. The next figures will therefore represent the evolution of single Fourier modes.

Figure 5 represents the slow start of convection which was described above by linear theory. This figure shows the ra-

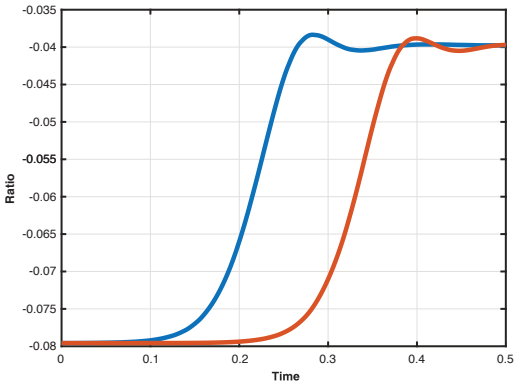

FIG. 5. This figure shows how nonlinearity changes the purely exponential growth of very small initial amplitudes, for the hand-picked case where the initial amplitude ratio B_0/A_0 is fixed according to eq. (47) The plots show the evolution of the ratio of $A_{11}(t)/C_{11}(t)$ for $R = 32\pi^4$ and $Pr = 1$, utilizing the spectral analysis.
Blue curve: $\theta(x,y,0) = 0.01\cos(\pi x)\sin(\pi y)$,
$\psi(x,y,0) = -0.01 \times 4\pi\sin(\pi x)\sin(\pi y)$,
$\omega(x,y,0) = -0.01 \times 8\pi^3\sin(\pi x)\sin(\pi y)$.
Red curve: $\theta(x,y,0) = 0.001\cos(\pi x)\sin(\pi y)$,
$\psi(x,y,0) = -0.001 \times 4\pi\sin(\pi x)\sin(\pi y)$,
$\omega(x,y,0) = -0.001 \times 8\pi^3\sin(\pi x)\sin(\pi y)$.

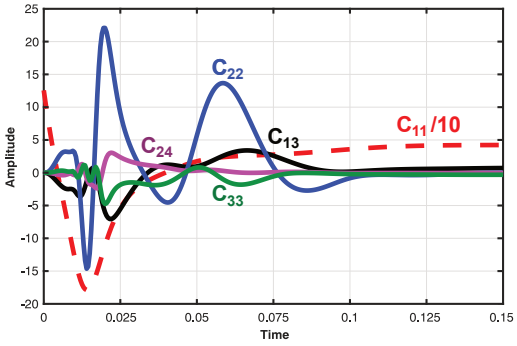

FIG. 6. Evolution of individual Fourier components C_{ij} for the streamfunction $\psi(x,y,t)$ referring to eq. (95) for $R = 8R_c = 64\pi^4$ and $Pr = 1$. The red dotted line are added representing the fundamental component $C_{11}(t)$ scaled by dividing it by 10. Initial conditions are as follows: $\theta(x,y,0) = 10\cos(\pi x)\sin(\pi y)$, $\psi(x,y,0) = 40\pi\sin(\pi x)\sin(\pi y)$, $\omega(x,y,0) = 80\pi^3\sin(\pi x)\sin(\pi y)$.

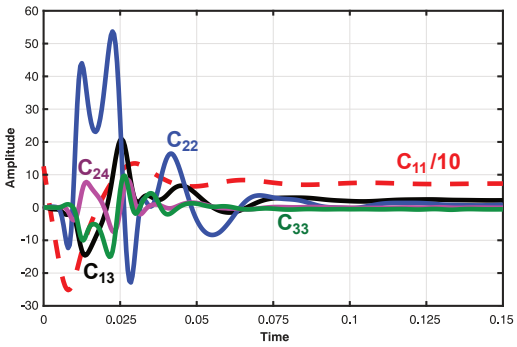

FIG. 7. Evolution of individual Fourier components C_{ij} for the streamfunction $\psi(x,y,t)$ referring to eq. (95) for $R = 16R_c = 128\pi^4$ and $Pr = 1$. The red dotted line are added representing the fundamental component $C_{11}(t)$ scaled by dividing it by 10. Initial conditions are as follows: $\theta(x,y,0) = 10\cos(\pi x)\sin(\pi y)$, $\psi(x,y,0) = 40\pi\sin(\pi x)\sin(\pi y)$, $\omega(x,y,0) = 80\pi^3\sin(\pi x)\sin(\pi y)$.

tio $A_{11}(t)/C_{11}(t)$ between the thermal mode and streamfunction mode, as they start from very small amplitudes. The initial amplitude ratio is chosen carefully according to eq. (47), which specifies the case where the preferred thermal mode and the associated flow mode will grow with identical growth rates according to linear theory of instability. Thereby Figure 5 reveals how linear theory breaks down, which happens when this ratio is no longer constant. Two cases of slow start are shown, where the slowest case has amplitudes a factor 10 lower than the other less slow case.

Figures 6 and 7 show the evolution of a variety of spectral components for the streamfunction, giving a qualitative confirmation of our small-time expansion for the kick-started supercritical convection. The Prandtl number $Pr = 1$ is chosen since the above theory suggests that it is optimal for triggering higher Fourier modes of motion from a single-mode initial state.

We display the spectral components C_{ij} for the streamfunction (or equivalently those for the vertical velocity $B_{ij} = -i\pi C_{ij}$). C_{11} is the unstable mode included in the initial condition. From the above theory, we recall that the Fourier mode C_{13} emerged in the third-order solution of the small-time expansion for the kick-start. The fourth-order solution made two new Fourier modes C_{22} and C_{24} appear. Figures 6 and 7 show the evolution of all Fourier modes with non-negligible amplitudes that are three times or less superharmonics of the leading mode in each direction. The only significant mode which was not detected by our small-time expansion to order t^4 is C_{33}, but we note that it starts very slowly, which it should.

The numerical experiments of kick-starting the convection were carried out in accordance with our analytical findings, where the intention was to trigger higher modes that could interact with one another as a route to chaos. The initial flow and initial temperature were chosen with contrasting values, far from their joint steady state. Yet, the results show that there is only a short transient stage of escalating complexity before the process is reversed so that steady convection can be established.

Figure 8 illustrates how our designed initial conditions can develop early spiral patterns in the vertical plane for two-

dimensional convection. This is a visualization of the process represented by its spectral components in Figure 7. It is the kick-start with opposite directions of initial spin and initial buoyancy torque that results in the most complex transient temperature field. The process shown in Figure 8 goes through two flow reversals, which means that the final steady state regains the initial direction of the net spin in the square cavity. Kick-starting the supercritical convection leads to flow reversals at Rayleigh numbers much lower than those reported for similar phenomena (see Podvin and Sergent[25]).

Figure 8 starts with an early stage where the initial counterclockwise spin is rapidly being reversed. The next stage is a gradual development of fine structured isotherms with increasing clockwise spin until diffusion begins wiping out the spiral patterns while the clockwise spin falls to zero. After that, a final steady state with slow counter-clockwise spin establishes. There is no periodicity, shown by the irregular transient behavior of the higher Fourier modes for the streamfunction displayed in Figure 7.

The streamline pattern does not change significantly while the isotherms exhibit transient spirals during flow reversal. Spiraling convection patterns in the horizontal plane are mentioned in the literature[26], while transient spirals in spatially diffusing and mutually reacting chemical substances are known from the Belousov-Zhabotinsky reaction[2].

VII. ON INTEGRATED PHYSICAL QUANTITIES

Improved physical understanding may be gained from studying the evolution of certain macroscopic parameters. The analytical theory has limited possibilities other than identifying some early trends. We will now consider physical quantities involving vorticity and heat transport.

A. Generation and decay of integrated vorticity

Vorticity is not conserved in this transient thermomechanical process. In linear theory, we have seen how vorticity can be initiated from a motionless state of the purely thermal initial field when the Rayleigh number is supercritical. We have also seen how an initial vorticity field can initiate a thermal perturbation from an initially isothermal state. We have investigated the sensitivity of the early nonlinear process with respect to different combinations of initial conditions.

Let us derive a basic theorem for the integrated vorticity. The nonlinear vorticity equation (8) is first rewritten as

$$\frac{\partial \omega}{\partial t} = -\nabla\cdot(\omega\vec{v}) + PrR\frac{\partial \theta}{\partial x} + Pr\nabla^2\omega, \tag{96}$$

taking the Boussinesq approximation of incompressible flow into account. We integrate this equation over the square area and apply Green's theorem

$$\frac{d}{dt}\int_0^1\int_0^1 \omega dxdy = Pr\int_\Gamma (R\theta\vec{i} + \nabla\omega)\cdot d\vec{L} \tag{97}$$

This area integral of the vorticity may be called the net spin. Γ denotes the contour for counterclockwise line integral around the square, where $d\vec{L}$ is the curve element. The contribution from the convected vorticity is absent in eq. (97) because $\vec{v}\cdot d\vec{L} = 0$ along the impermeable contour of the cavity. This integral is developed to the following theorem for evolution of net spin in the square cavity

$$\frac{d}{dt}\int_0^1\int_0^1 \omega(x,y,t)dxdy = PrR\int_0^1(\theta(1,y,t)-\theta(0,y,t))dy + Pr\int_\Gamma \nabla\omega(x,y,t)\cdot d\vec{L}. \tag{98}$$

Here we see that the only mechanism that can increase the net spin is the buoyancy torque along the vertical sidewalls, expressed by the temperature perturbations there. This mechanism is strong for Prandtl numbers greater than one, whereby buoyancy will suppress a fragmentation of the leading modes by transient nonlinear vortex interactions. Even for mercury with $Pr = 0.025$, the factor PrR will be quite large, around 20 for slightly supercritical convection. This means that buoyancy will always be important. A supercritical thermomechanical flow will never become completely dominated by vortex interactions, as the vortices will remain in nonlinear feedback with their temperature perturbations.

The last integral in eq. (98) will always reduce the net spin. This integral along the entire contour Γ represents the viscous dissipation prescribed by the Navier-Stokes equation.

The kinetic energy is not conserved in the transient flow. It is likely that the kinetic energy will increase exponentially as long as the preferred mode is essentially the only Fourier component of motion. Once there is one more Fourier mode present, we expect it to steal some of the net spin of the leading mode.

The sign of the first higher Fourier mode of motion $\sin(\pi x)\sin(3\pi y)$ gives an immediate qualitative check of these arguments. The net spin of this mode may be considered as concentrated in the subdomain $0<x<1,\ 0<y<1/3$, since the remaining domain $0<x<1,\ 1/3<y<1$ has zero net spin as a full spatial period in the vertical direction. The solution (74) reveals that the Fourier contribution to ω_3 of the type $\sin(\pi x)\sin(3\pi y)$ has a negative sign, confirming that it reduces the net spin. It has to behave in this manner in order to avoid a rapid rise in kinetic energy when there is no additional energy source available.

Figure 9 shows how the integrated vorticity varies with time for kick-started convection. Two cases with the standard value $Pr = 1$ are represented, but two additional plots complement them with the same initial conditions and a lower Prandtl number $Pr = 0.2$. Thereby we illustrate that an efficient triggering of early flow reversals needs a Prandtl number of order one, where buoyancy torque and initial spin are comparable and can be in mutual conflict. A small Prandtl number provides the initial unicellular flow with an angular momentum not overcome by buoyancy forces, because heat diffusion is too strong.

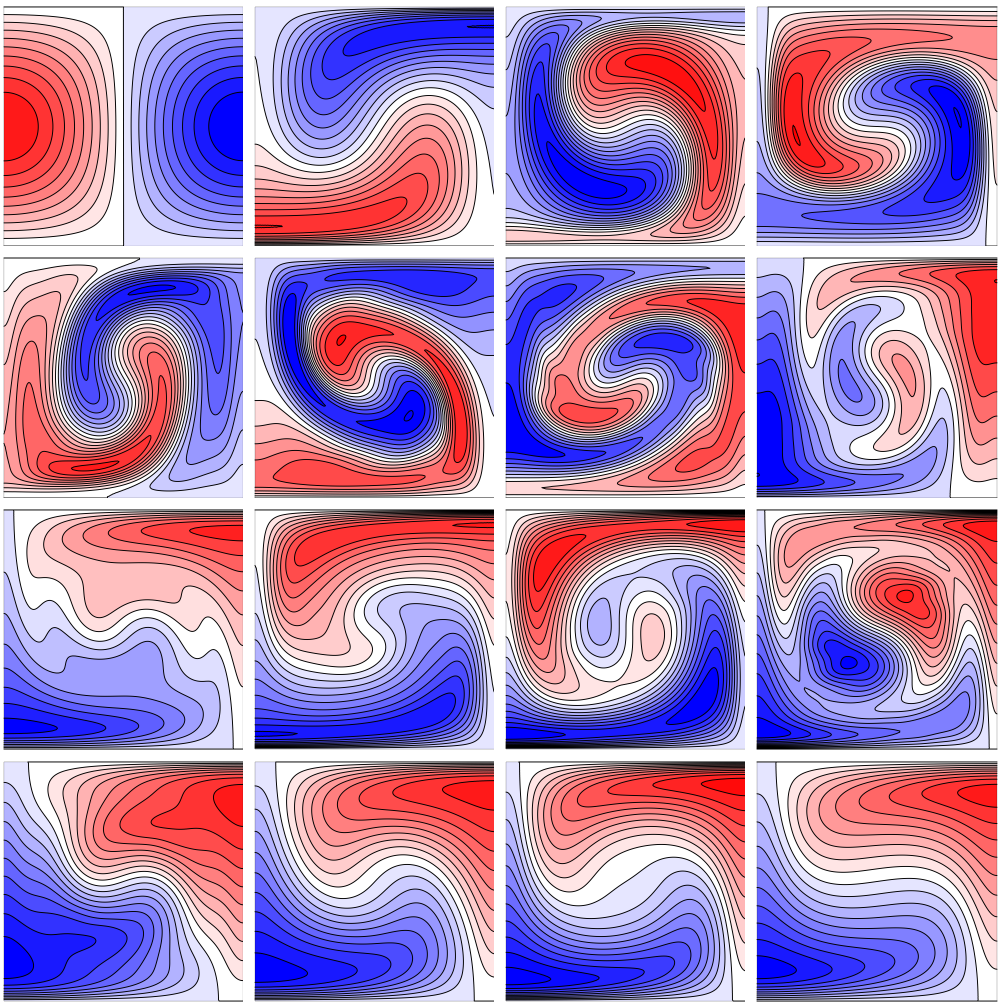

FIG. 8. Evolution of the temperature perturbation $\theta(x,y,t)$ for $R = 16R_c = 128\pi^4$ and $Pr = 1$ with constant time steps, $t = 0$, 0.0025, 0.005, 0.0075, 0.01, 0.0125, 0.015, 0.0175, 0.02, 0.0225, 0.025, 0.0275, 0.03, 0.0325, 0.035, respectively, and then finally, 0.3 (stationary value). Initial conditions are as follows: $\theta(x,y,0) = 10\cos(\pi x)\sin(\pi y)$, $\psi(x,y,0) = 40\pi\sin(\pi x)\sin(\pi y)$, $\omega(x,y,0) = 80\pi^3\sin(\pi x)\sin(\pi y)$. The same-sign initial amplitudes for kick-started streamfunction and temperature cause an apparent early evolution of complexity. Our designed conflicting directions for the buoyancy torque versus initial spin will develop fine structures in temperature combined with a couple of non-periodic flow reversals. Strict constraints of symmetry prevent chaos from evolving, where temporarily emerging fine structures are reversed by dissipation so that a final steady state is settled.

B. On the heat transport

With the chosen boundary conditions, the entire heat transport between the square cavity and its surroundings takes place through the lower and upper boundaries $y = 0$ and $y = 1$ (in the dimensionless description). The heat transfer is represented by Nusselt numbers $Nu_0(t)$ and $Nu_1(t)$ for the lower

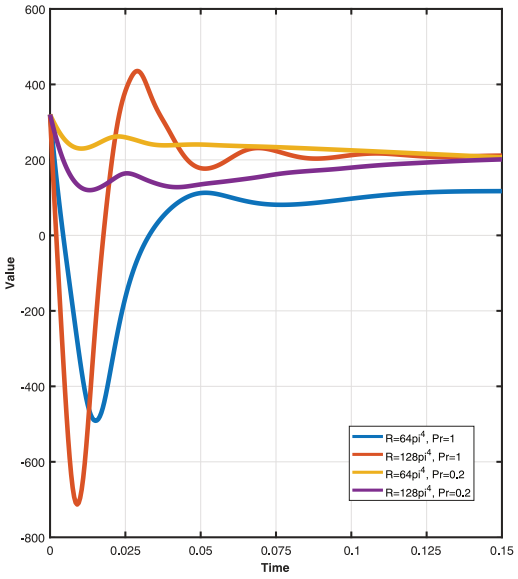

FIG. 9. Evolution of the integrated vorticity over the square $(\int_0^1\int_0^1 \omega(x,y,t)dxdy$, referring to eq. (98)), given for different R and Pr. We show four combinations, which also illustrate the effects of smaller Prandtl number: $R = 64\pi^4$ or $R = 128\pi^4$ combined with $Pr = 1$ or $Pr = 0.2$. The same initial conditions are chosen for all cases, given as follows: $\theta(x,y,0) = 10\cos(\pi x)\sin(\pi y)$, $\psi(x,y,0) = 40\pi\sin(\pi x)\sin(\pi y)$, $\omega(x,y,0) = 80\pi^3\sin(\pi x)\sin(\pi y)$.

and upper plane, respectively. The definitions are

$$Nu_0(t) = 1 - \int_0^1 \left.\frac{\partial\theta}{\partial y}\right|_{y=0} dx, \tag{99}$$

$$Nu_1(t) = 1 - \int_0^1 \left.\frac{\partial\theta}{\partial y}\right|_{y=1} dx. \tag{100}$$

These Nusselt numbers represent the total heat transport divided with the transport due to thermal conduction alone.

Figure 10 shows the evolution of the Nusselt number for some previous cases of computations with $Pr = 1$. We add two cases where $Pr = 0.2$. We have calculated the two versions of the Nusselt number separately, but they are always identical, which is a result of the flow symmetry, which we investigate in the Appendix. This flow symmetry is a basic constraint preventing that chaos is able to evolve. We note the huge amplitudes in the transient heat transfer. In all the displayed cases, the early heat flux will even go downward, with negative Nusselt number. We recall that pure conduction has unit Nusselt number. It is the designed early spin in the opposite direction of the buoyancy torque which forces the Nusselt number to be temporarily negative until buoyancy overcomes this kick-start and establishes a final steady state.

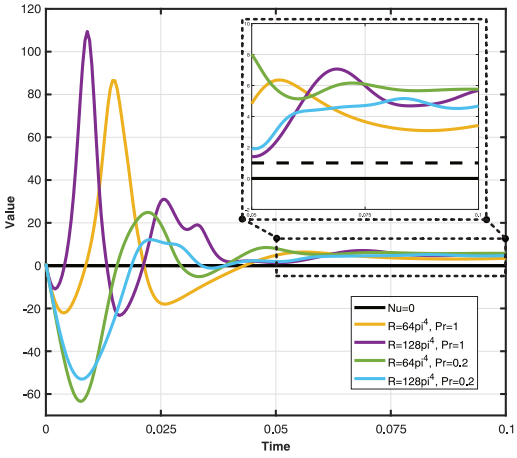

FIG. 10. Evolution of the heat transfer through the boundaries. This is represented by the Nusselt numbers $Nu_0(t)$ and $Nu_1(t)$, referring to eqs. (99) and (100) with different choices for R and Pr. The initial conditions are the same for all cases, chosen as follows: $\theta(x,y,0) = 10\cos(\pi x)\sin(\pi y)$, $\psi(x,y,0) = 40\pi\sin(\pi x)\sin(\pi y)$, $\omega(x,y,0) = 80\pi^3\sin(\pi x)\sin(\pi y)$.

Figure 10 shows that very large positive Nusselt numbers may occur during the transient prosess before the steady state settles. These dramatic nonlinear effects in the early heat transport take place at moderate Rayleigh numbers. Similar phenomena are mostly known from turbulent convection at much higher Rayleigh numbers[27].

Figure 10 shows the same initial values for the four different choices of Rayleigh numbers and Prandtl numbers. In Figure 11, we fix these key parameters at $R = 8R_c$ and $Pr = 1$ for studying how different choices of initial amplitudes affect the two leading spectral components for the temperature. These are A_{11}, which is the only one with a nonzero initial value, and A_{02}, which is the leading Fourier term that takes care of the heat flux through the boundaries.

VIII. SUMMARY AND CONCLUSIONS

The present model picks the preferred modes of linear stability to compose the initial state of supercritical Rayleigh-Bénard convection to evolve with full nonlinearity. We put aside all stability considerations for the nonlinear convection to focus entirely on the evolution from a given initial state. Sensitivity with respect to the initial conditions may serve as a substitute for stability. In our problem, we have two independent initial values, allowing variety as well as complexity in the early transient evolution. Our computations show that the final state is always steady and independent of the initial values, but this result is linked to our choice of a square cavity.

We have found that strict symmetry constraints set by the

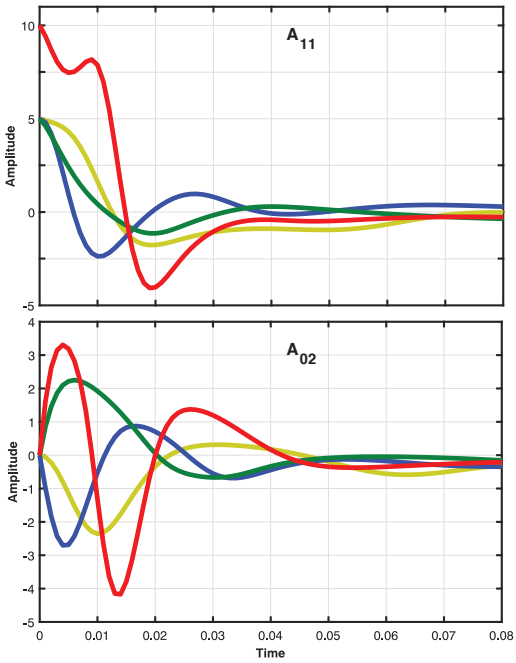

FIG. 11. Evolution of two thermal Fourier components with different intial conditions for $R = 64\pi^4$ and $Pr = 1$. The upper subfigure represents $A_{11}(t)$, while the lower subfigure represents $A_{02}(t)$.
Yellow curve: $\theta(x,y,0) = 5\cos(\pi x)\sin(\pi y)$,
$\psi(x,y,0) = 0$,
$\omega(x,y,0) = 0$.
Blue curve: $\theta(x,y,0) = 5\cos(\pi x)\sin(\pi y)$,
$\psi(x,y,0) = -40\sin(\pi x)\sin(\pi y)$,
$\omega(x,y,0) = -80\pi^2\sin(\pi x)\sin(\pi y)$.
Green curve: $\theta(x,y,0) = 5\cos(\pi x)\sin(\pi y)$,
$\psi(x,y,0) = 40\sin(\pi x)\sin(\pi y)$,
$\omega(x,y,0) = 80\pi^2\sin(\pi x)\sin(\pi y)$.
Red curve: $\theta(x,y,0) = 10\cos(\pi x)\sin(\pi y)$,
$\psi(x,y,0) = 40\sin(\pi x)\sin(\pi y)$,
$\omega(x,y,0) = 80\pi^2\sin(\pi x)\sin(\pi y)$.

initial conditions block the process of successive vortex interactions by stopping their fragmentation, while the initial spin may be reversed a couple of times before the final steady flow is established. The flow based on initially preferred modes for a square cavity is always unicellular and shows very little variation in its streamline patterns during the non-periodic variation of the flow amplitude.

Vortex interactions can be triggered from an elementary initial state of preferred eigenfunctions for the onset problem. The most efficient procedure is to kick-start the convection with relatively large initial amplitudes for the flow and for the temperature perturbation. We are able to design a conflict between the initial angular momentum of the unicellular flow and the initial thermal buoyancy torque from the initial temperature field. We have not found a simple physical explanation of the couple of flow reversals that may occur before the time-dependence fades and a steady-state nonlinear convection establishes. The flow is never dominated by inertia, otherwise the buoyancy torque could not overcome the initial spin for the first reversal to take place. It is fascinating that a second flow reversal may occur, with inertia seemingly striking back to restore the initial direction of rotation. This phenomenon is related to the emergence and later decay of spiralling isotherms.

There are severe constraints for the early vortex interactions.

(i) The single-pair of thermomechanical modes for initiation of the supercritical convection gives strict constraints of symmetry which stops the early triggering of higher Fourier modes and lets a steady supercritical flow establish. The present model with single-mode initiation has a strict antisymmetry for the perturbation temperature, and a strict symmetry for the instantaneous streamline pattern.

(ii) The triggering of vortex interactions is indirect because it is not exclusively mechanical. It needs nonlinear heat transport to emerge, with feedback to the vorticity equation through the buoyancy term.

(iii) The Prandtl number (Pr) cannot be too small for the buoyancy term to be effectively feeding higher modes of motion in the vorticity equation. The Prandtl number cannot be too large to avoid that the diffusion of vorticity stops the transient vortex interactions. We have given priority to the choice $Pr = 1$ for demonstrating the transient phenomena of nonlinear convection since this case represents a balance of inertia versus buoyancy.

We have derived a theorem for the evolution of integrated vorticity, from which we conclude that the transient process becomes dominated by buoyancy at the expense of inertia. The fact that the sign of the net spin may change at least two times during the nonlinear transient process shows that a sufficiently strong buoyancy torque will overcome the initial spin of the unicellular initial flow. Moreover, it also shows that the initial spin may be able to strike back to reestablish its initial direction. A well-known fact from linear theory is that the eigenfunctions for vertical velocity and temperature are identical. However, any nonlinear convection with supercritical Rayleigh numbers will disturb a symmetry between the vertical velocity and the temperature perturbation. With nonlinearity, a distinct class of thermal Fourier modes without horizontal dependency emerges. These thermal modes do not have any counterpart for the vertical flow, forming a genuinely nonlinear asymmetry between temperature and vertical velocity. This asymmetry seems to underpin the aperiodic thermomechanical bounce back of flow reversals.

Large-scale flow reversals are an important phenomenon in two-dimensional chaotic convection at very high Rayleigh numbers[28]. In these numerical simulations[28], a soft start from initial small-amplitude noise was applied. Our type of reversal can only happen when the convection is kick-started with large amplitudes where the initial buoyancy torque is opposing the initial spin. We have not been able to find more than

two flow reversals in our model of laminar convection at moderate Rayleigh numbers.

The present approach aims at an improved causal understanding of convection at small Prandtl numbers and moderately supercritical Rayleigh numbers. The initial state must be richer than the present one before we can link the present model to the classical work by Busse[29]. The present model does not allow any periodic oscillations to establish.

The present work is a well-ordered minimalist approach to strongly nonlinear transient convection with small and moderate Prandtl numbers. We have avoided arbitrary noise as a substitute for causation of flow structures. We found that vortex interactions could only emerge by being aided by thermal perturbations. After that, they did not escalate but were strongly impeded and faded by diffusion. Follow-up work should focus on richer initial states, where the strict symmetries that we have demonstrated numerically (and shown analytically in the Appendix) are dismantled in a gradual and controlled manner.

The present work aims at a simplistic yet first-principle approach to the classical Rayleigh-Bénard problem with finite amplitude. We have provided a link from our model to the classical Lorenz model, which is discussed in the monograph by Strogatz[30]. In comparison, our reduced Lorentz-type model represents the physical processes of Rayleigh-Bénard convection more closely than the classical model. Our reduced model does not give a much-improved understanding because too great complexities remain in our truncated set of ordinary differential equations. Only our full model may serve to exemplify phenomena of continuum physics to be classified within the general theory of nonlinear dynamical systems[31]. A full physical model with partial differential equations is more specialized and restricted than the theory of dynamical systems based on coupled sets of difference equations and ordinary differential equations.

Appendix A: On symmetries posed by the initial conditions

In this appendix we will expose the mathematical symmetries in this initial condition, which give constraints for the further evolution. We postulate that the temperature field during its evolution has the form

$$\theta(x,y,t) = \sum_{m=1}^{\infty}\sum_{n=1}^{\infty} A_{mn}(t)\cos(m\pi x)\sin(n\pi y), \quad \text{where } m+n \text{ is an even number.} \tag{A1}$$

For this postulate to be valid, it is necessary that it holds at $t = 0$. Our choice of initial temperature field is

$$\theta(x,y,0) = A_{11}(0)\sin(\pi x)\sin(\pi y), \tag{A2}$$

so that $m+n = 2$, which makes the postulate hold for the initial state.

Similarly, we postulate that the streamfunction during its evolution has the form

$$\psi(x,y,t) = \sum_{p=1}^{\infty}\sum_{q=1}^{\infty} C_{pq}(t)\sin(p\pi x)\sin(q\pi y), \quad \text{where } p+q \text{ is an even number.} \tag{A3}$$

Our choice of initial flow field is

$$\psi(x,y,0) = C_{11}(0)\sin(\pi x)\sin(\pi y), \tag{A4}$$

so that $p+q = 2$, which makes the postulate hold for the initial state.

In order to verify the combined symmetry postulate for the temperature and flow fields, these Fourier series solutions are inserted into the nonlinear equations (8) - (9), to check whether the formulas for $\partial\theta/\partial t$ and $\partial\psi/\partial t$ have the same form as the form postulated for θ and ψ, respectively. The linear terms in the governing equations (8) - (9) will automatically satisfy this requirement.

We only need to look at the nonlinear terms to check whether the postulate holds. The heat equation (9) has the convective heat transport term $\vec{v}\cdot\nabla\theta$ which gives rise to the following combinations of Fourier terms

$$\cos((m\pm p)\pi x)\sin((n\pm q)\pi y). \tag{A5}$$

We have postulated that

$$m+n = 2M, \quad p+q = 2N, \tag{A6}$$

where we introduce the notation $2M$ and $2N$ for two even numbers (where M and N may be arbitary integers).

As far as the heat equation (9) is concerned, the postulate holds if all four combinations of the sums $(m\pm p)+(n\pm q)$ are even numbers. Inserting the postulated relationships (A6) for each of these four combinations leads to the formulas

$$\begin{aligned} m-p+n-q &= 2(M-N),\\ m+p+n-q &= 2(M-N+p),\\ m-p+n+q &= 2(M-N+q),\\ m+p+n+q &= 2(M-N+p+q). \end{aligned} \tag{A7}$$

Since M, N, p and q are integers, the right hand side of each equation is an even number. Thereby we have confirmed that $\partial\theta/\partial t$ has the same form as that postulated by $\theta(x,y,t)$ according to eq. (A1).

We omit the analogous argument to show that $\partial\psi/\partial t$ has the same form as that postulated by $\psi(x,y,t)$ according to eq. (A3).

When we start from the given initial states (A2) and (A4) and integrate in time these two coupled functions $\theta(x,y,t)$ and $\psi(x,y,t)$, these two functions will by induction keep their postulated forms (A1) and (A3). These two functions obey strict but opposite symmetries with respect to the mid-point $(x,y) = (1/2, 1/2)$ of the square cavity.

The above argumentation by induction is not a proof in the strict mathematical sense since the successive induction applies infinitesimal time steps, while induction as a mathematical concept is established for finite steps only. Rigorous proof

for the combined symmetry/antisymmetry can be developed by group theory[31]. Support for the antisymmetry of the supercritical temperature field is given by our numerical simulations.

The streamline pattern $\psi(x,y,t)$ is symmetric with respect to the mid-point at all times

$$\psi(x,y,t) = \psi(1/2-x,1/2-y,t), \;\; t>0. \qquad \text{(A8)}$$

The simultaneous behavior of the temperature perturbation $\theta(x,y,t)$ is that it is anti-symmetric with respect to the mid-point

$$\theta(x,y,t) = -\theta(1/2-x,1/2-y,t), \;\; t>0. \qquad \text{(A9)}$$

We have now established the two opposite and mutually dependent symmetries for the flow field and temperature field. These symmetries arose by being selected for the initial modes, and they are maintained by being preserved by the governing equations. The initial fields are equal to the pair of preferred eigenfunctions for the square cavity. In the general nonlinear initial value problem, these initial modes can be given independent amplitudes, as demonstrated in the main text.

DATA AVAILABILITY

The data that support the findings of this study are available from the corresponding author upon reasonable request.

REFERENCES

[1]A. M. Turing, "The chemical basis of morphogenesis," Philos. Trans. R. Soc. London. Ser. B: Biolog. Sci. **237**, 37–72 (1952).
[2]I. Prigogine and I. Stengers, *Order out of Chaos: Man's new dialogue with nature* (Bantam Books, 1984).
[3]J. W. S. Lord Rayleigh, "On convection currents in a horizontal layer of fluid, when the higher temperature is on the under side," The London, Edinburgh, and Dublin Philos. Mag. & J. Sci. **32**, 529–546 (1916).
[4]W. Malkus and G. Veronis, "Finite amplitude cellular convection," J. Fluid Mech. **4**, 225–260 (1958).
[5]S. Chandrasekhar, "Hydrodynamic and hydromagnetic stability," (Clarendon Press, Oxford 1961).
[6]D. Moore and N. Weiss, "Two-dimensional Rayleigh-Bénard convection," J. Fluid Mech. **58**, 289–312 (1973).
[7]E. Palm, "Nonlinear thermal convection," Ann. Rev. Fluid Mech. **7**, 39–61 (1975).
[8]F. H. Busse and R. Clever, "Transitions to complex flows in thermal convection," Archiwum Mechaniki Stosowanej **43**, 565–575 (1991).
[9]P. G. Drazin and W. H. Reid, *Hydrodynamic stability* (Cambridge university press, 2004).
[10]A. Schlüter, D. Lortz, and F. Busse, "On the stability of steady finite amplitude convection," J. Fluid Mech. **23**, 129–144 (1965).
[11]J. Wesfreid, Y. Pomeau, M. Dubois, C. Normand, and P. Bergé, "Critical effects in Rayleigh-Bénard convection," J. de Physique **39**, 725–731 (1978).
[12]A. C. Newell and J. A. Whitehead, "Finite bandwidth, finite amplitude convection," J. Fluid Mech. **38**, 279–303 (1969).
[13]C. Normand, Y. Pomeau, and M. G. Velarde, "Convective instability: a physicist's approach," Rev. Modern Phys. **49**, 581 (1977).
[14]Y. Pomeau and P. Manneville, "Stability and fluctuations of a spatially periodic convective flow," J. de Physique Lettres **40**, 609–612 (1979).
[15]E. Bodenschatz, W. Pesch, and G. Ahlers, "Recent developments in Rayleigh-Bénard convection," Ann. Rev. Fluid Mech. **32**, 709–778 (2000).
[16]P. Cerisier, H. N. Thi, and B. Billia, "Disorder dynamics of arrays in bénard convection," Physica D: Nonlinear Phenomena **61**, 113–118 (1992).
[17]E. L. Koschmieder, *Bénard cells and Taylor vortices* (Cambridge University Press, 1993).
[18]M. Bestehorn and H. Haken, "A calculation of transient solutions describing roll and hexagon formation in the convection instability," Phys. Lett. A **99**, 265–267 (1983).
[19]J. P. Whitehead and C. R. Doering, "Ultimate state of two-dimensional Rayleigh-Bénard convection between free-slip fixed-temperature boundaries," Physical Rev. Letters **106**, 244501 (2011).
[20]B. Wen, D. Goluskin, M. LeDuc, G. P. Chini, and C. R. Doering, "Steady Rayleigh-Bénard convection between stress-free boundaries," J. Fluid Mech. **905** (2020).
[21]E. Palm, "On the tendency towards hexagonal cells in steady convection," J. Fluid Mech. **8**, 183–192 (1960).
[22]F. H. Busse, "On the stability of two-dimensional convection in a layer heated from below," J. Math. Phys. **46**, 140–150 (1967).
[23]G. Hartung, F. H. Busse, and I. Rehberg, "Time-dependent convection induced by broken spatial symmetries," Physical Rev. Letters **66**, 2742 (1991).
[24]E. N. Lorenz, "Deterministic nonperiodic flow," J. Atmospheric Sci. **20**, 130–141 (1963).
[25]B. Podvin and A. Sergent, "Precursor for wind reversal in a square rayleigh-bénard cell," Physical Review E **95**, 013112 (2017).
[26]N. M. Ercolani, R. Indik, A. C. Newell, and T. Passot, "The geometry of the phase diffusion equation," J. Nonlinear Sci. **10**, 223–274 (2000).
[27]F. H. Busse and K. Heikes, "Convection in a rotating layer: a simple case of turbulence," Science **208**, 173–175 (1980).
[28]Q. Wang, S.-N. Xia, B.-F. Wang, D.-J. Sun, Q. Zhou, and Z.-H. Wan, "Flow reversals in two-dimensional thermal convection in tilted cells," J. Fluid Mech. **849**, 355–372 (2018).
[29]F. H. Busse, "The oscillatory instability of convection rolls in a low Prandtl number fluid," J. Fluid Mech. **52**, 97–112 (1972).
[30]S. H. Strogatz, "Nonlinear dynamics and chaos: with applications to physics," Biology, Chemistry and Engineering , 1 (1994).
[31]P. Chossat and R. Lauterbach, *Methods in equivariant bifurcations and dynamical systems*, Vol. 15 (World Scientific Publishing Company, 2000).

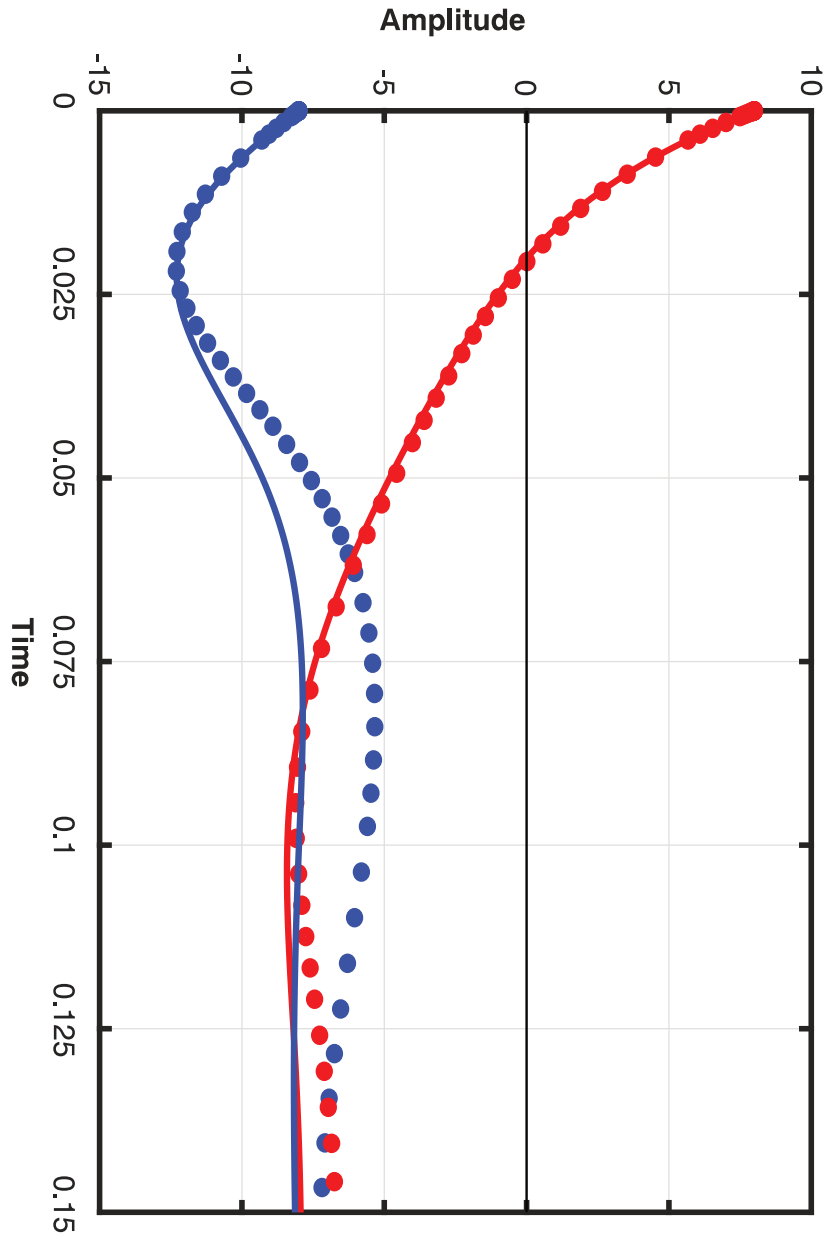

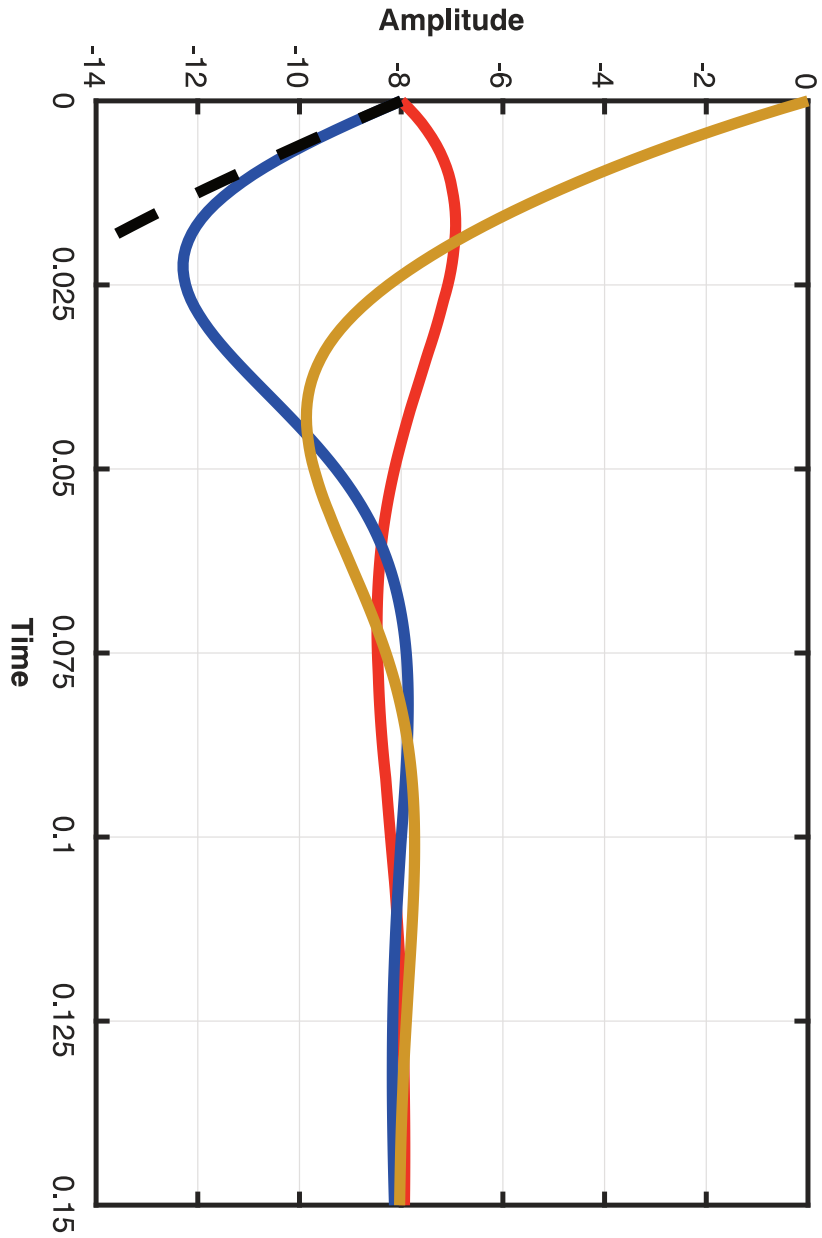

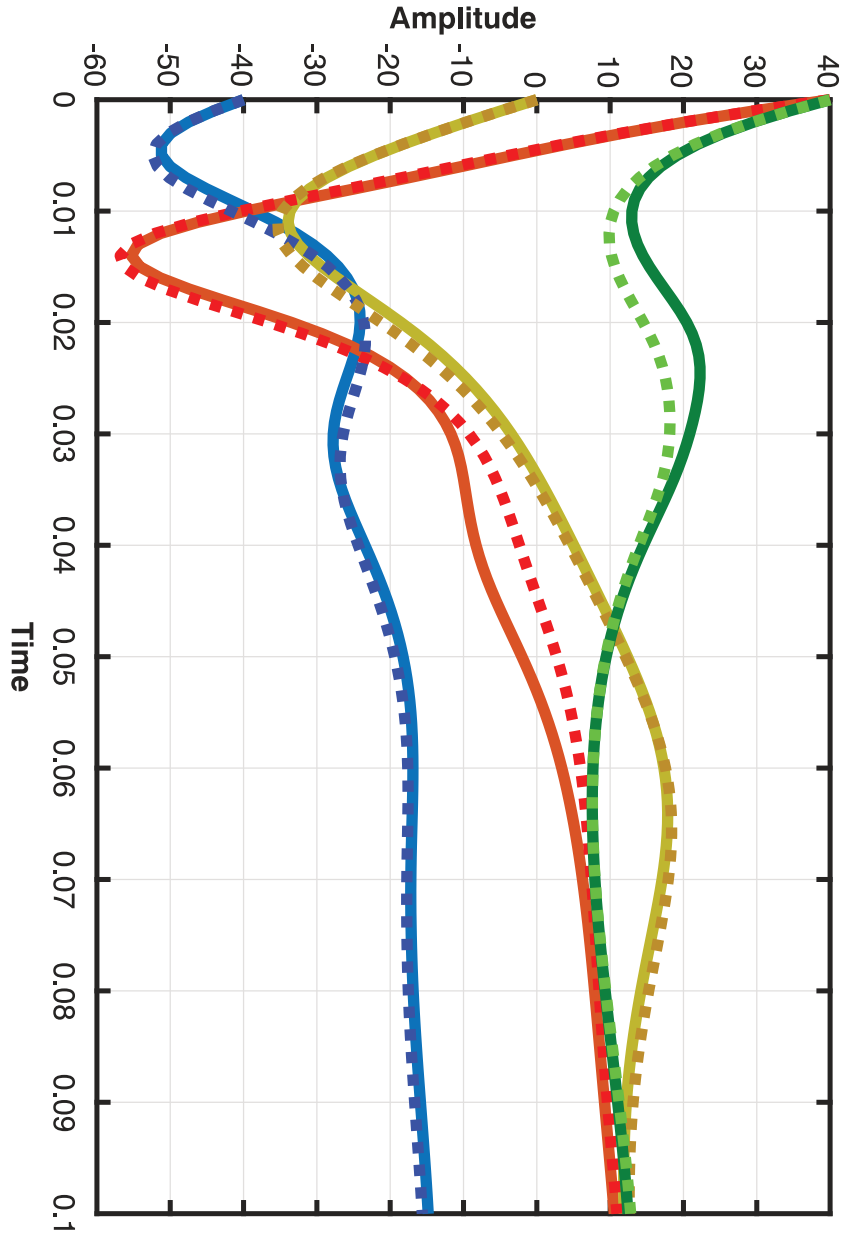

PLEASE CITE THIS ARTICLE AS DOI: 10.1063/5.0067546

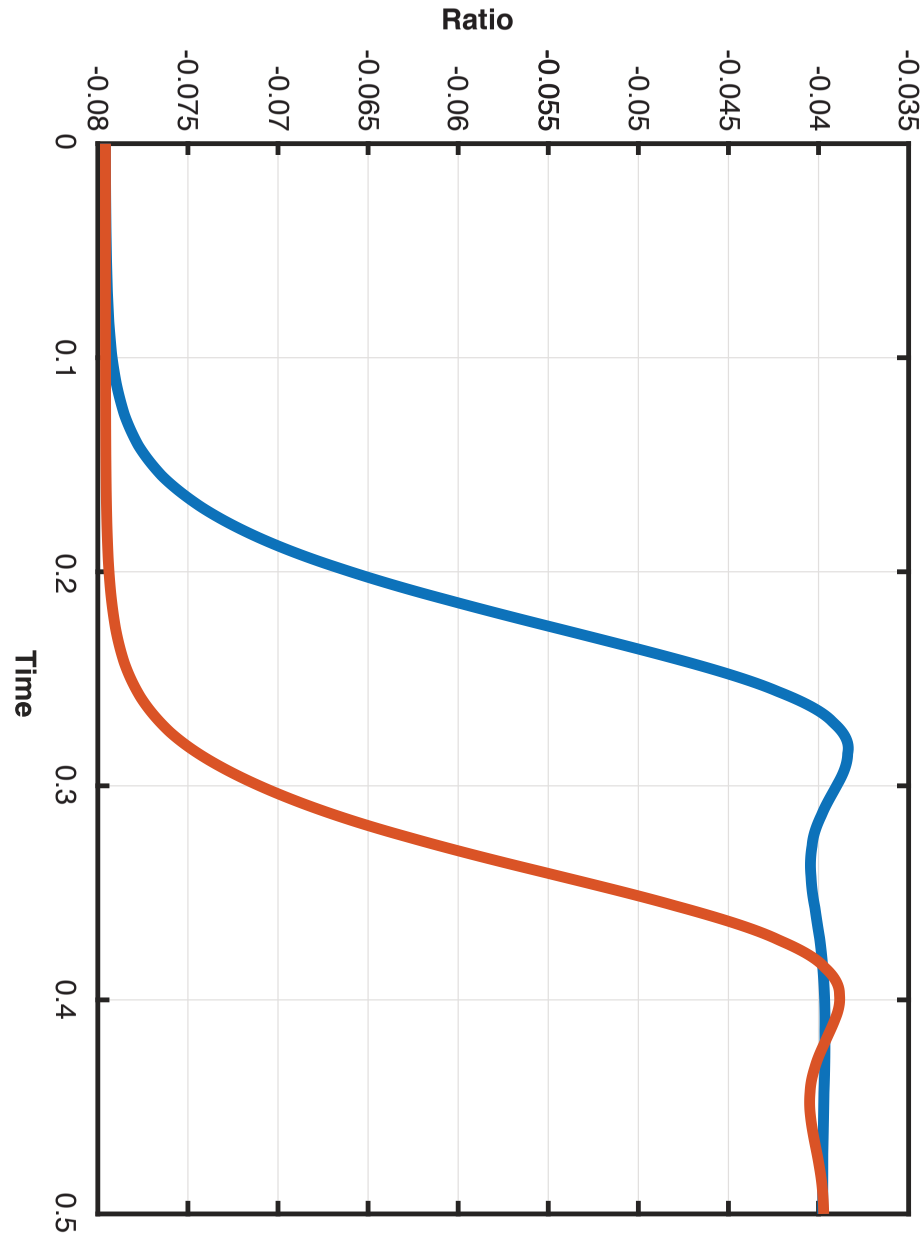

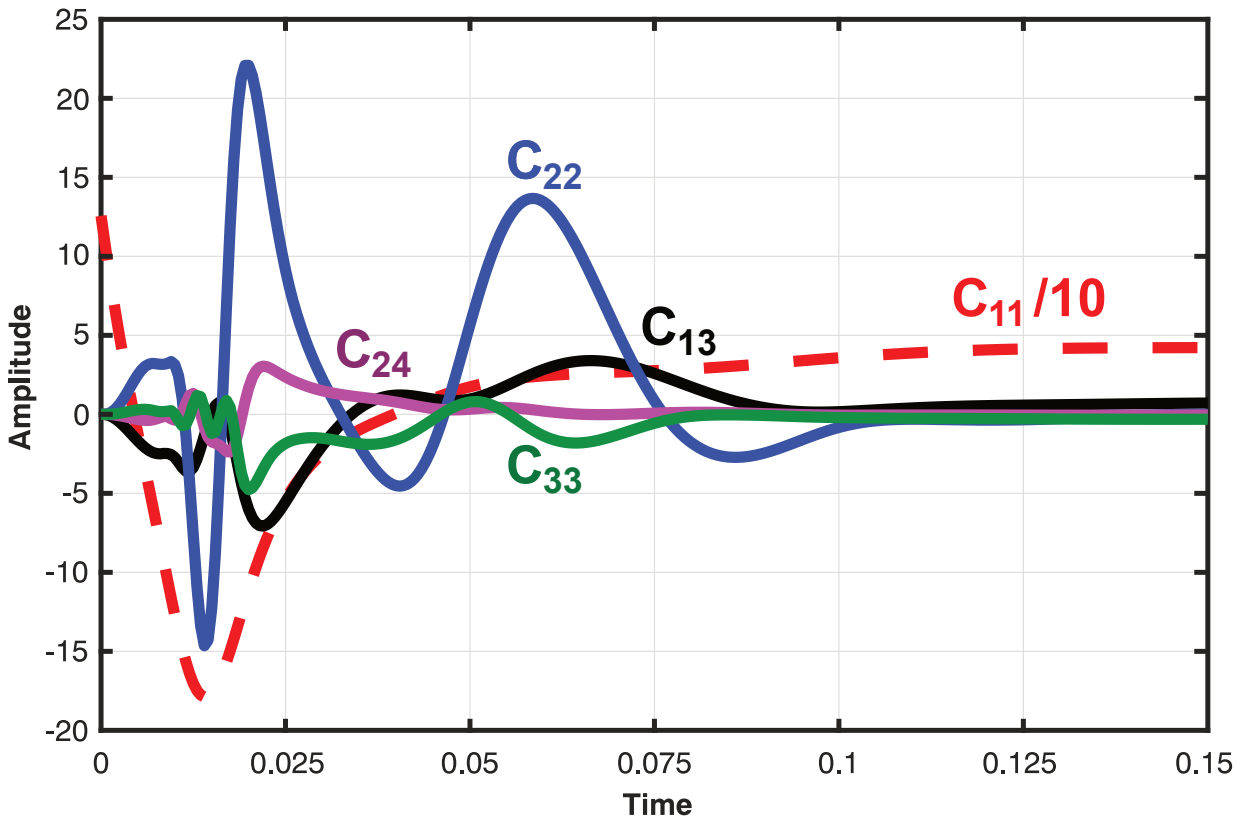

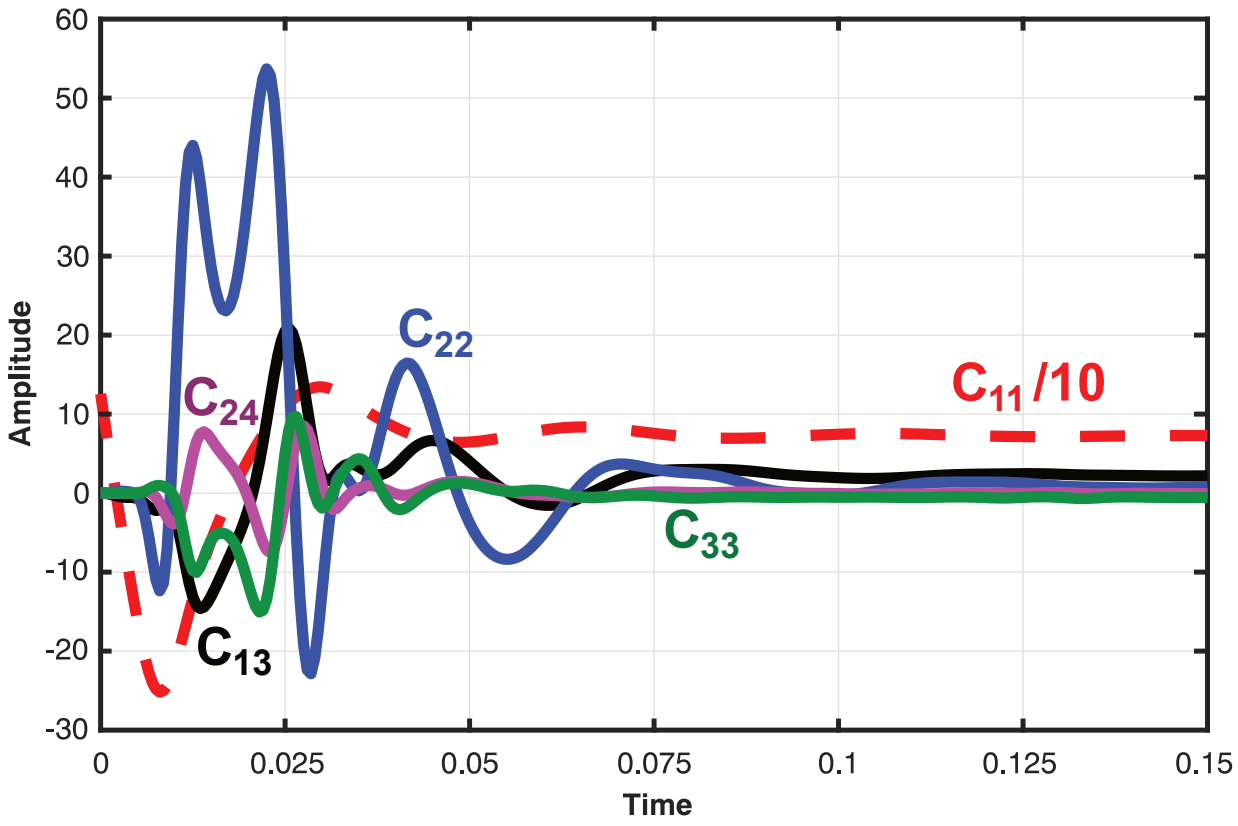

PLEASE CITE THIS ARTICLE AS DOI: 10.1063/5.0067546